Phosphine Ligands as Protecting Groups for 3*d* Complexes in Oxidation by O_2

Sarah E.N. Brazeau[a], Frances Pope[a], Vincent L. Huang[a], Clemens Anklin[b], Arnold L. Rheingold[c], Linda H. Doerrer[a,*]

[a] Department of Chemistry, Boston University, 590 Commonwealth Avenue, Boston, Massachusetts 02215

[b] Bruker BioSpin, 15 Fortune Drive, Billerica, Massachusetts 01821

[c] Department of Chemistry and Biochemistry, University of California, San Diego, 9500 Gilman Drive, La Jolla, California 92093

*Email address: doerrer@bu.edu

Abstract

A series of heteroleptic mixed phosphine/alkoxide 3*d* complexes was designed to evaluate PPh_3 as a protecting group, stabilizing the metal coordination sphere prior to O_2 exposure but oxidatively dissociating in the presence of O_2 to allow facile O_2 reduction by low coordinate metal centers. Complexes of the form $[(Ph_3P)_2M(OC_4F_9)_2]$ (M= Fe (**1**), Co (**2**), Ni (**3**), Zn (**4**)) and $[(Ph_3P)_2M(pin^F)]$ (M= Co (**8**), Ni (**9**), Zn (**10**) were prepared, along with related complexes with non-reactive L-donors, $[(DME)Fe(OC_4F_9)_2]$ (**5**) and $[(Ph_3PO)_2M(OC_4F_9)_2]$ (M= Fe (**6**), Ni (**7**)). Complexes were characterized by UV-vis and NMR spectroscopies, elemental analysis and single-crystal X-ray diffraction for **1**, **3**, **6**, **7**, **8**, **9**, and **10**. The electronic structure of **3** is particularly notable, with ~D_{4h} geometry at room temperature and ~T_d at low temperature, as determined by temperature dependent UV-vis and NMR (^1H, ^{31}P) spectroscopies. Complexes (M= Fe, Co, Ni) were screened for O_2 reactivity to assess the efficacy of PPh_3 as a protecting group. Dimeric $[Fe_2(\mu_2\text{-}O)(OPPh_3)_2(OC_4F_9)_4]$ (**13**) was isolated after O_2 reactivity with **1**, and characterized as described above. Related Fe complexes **5** and **6** were each combined with O_2 to generate intermediate species capable of both stoichiometric oxidase of hydroquinone to benzoquinone and sub-stoichiometric oxygen atom transfer of thioanisole (PhSMe) to methyl

phenyl sulfoxide. Fluorinated alkoxide ligand choice influenced O_2 reactivity in Co^{II} complexes, as reactivity was only seen in the less sterically hindering pin^F–containing complex **8**. In the Ni^{II} complexes, on the other hand, the particular fluorinated ligand was not a factor in O_2 reduction, as **3** and **9** exhibited similar reactivity. Related dimeric compounds $[Co_2(pin^F)_2(THF)_4)]$ (**11**) and $[Zn_2(pin^F)_2(THF)_2)]$ (**12**) were also isolated and characterized.

Keywords: fluorinated alkoxide, phosphine, oxidation, C-H bond, coordination number

Introduction

The desire to understand and improve upon oxidation catalytic transformations in Nature has led to the extensive investigation of reactivity of O_2 with 3*d* metal complexes. Fe and Cu are predominant in biological systems, and enzymes containing these metals activate O_2 for substrate oxidation.[1] Fe is present heme enzymes[2], including cytochrome P450 and chloroperoxidase, as well as in non-heme enzymes, examples including lipoxygenase, soluble methane monoxygenase, protocatechuate 3,4-dioxygenase, and toluene 4-monoxygenase.[3-6] Cu enzymes can perform oxidation reactions including oxidase (ascorbate, laccase), monooxygenase (tyrosinase, particulate methane monooxygenase), and dioxygenase (quercetin 2,3-dioxygenase).[7] Of particular interest at this moment is understanding the active sites of methane monooxygenases, in order to apply this knowledge to industrial settings. Complexes with either Fe or Cu in primarily N-donor ligand environments have been heavily investigated for reactivity with O_2, aiming to mimic the predominantly N-donor enzyme active site environments.[3, 4, 8-11] Promising CH_4 oxidation catalysts that do not have enzyme like cores are zeolites, porous aluminosilicate materials with either Cu or Fe.[12-19] The mechanism of CH_4 oxidation at these metal centers is also not fully understood.

To analyze the behavior of Cu in a fully O-donor environment, like that of Cu zeolites, our group has investigated Cu−O_2 reactivity with fully fluorinated linear Cu^I alkoxide moieties,[20] $\{Cu(OR)_2\}^-$ with perfluoro-*t*-butoxide and perfluoropinacolate (pin^F), as well as partially fluorinated alkoxides $OCMeMe^F_2$ and $OCPhMe^F_2$.[21-23] When reacted at low temperature with O_2, the fully fluorinated Cu^I complexes formed the trinuclear core $\{Cu_3(\mu_3\text{-}O)_2\}^{3-}$ at all concentrations, whereas this observation was concentration dependent for the partially fluorinated alkoxides. Although the monodentate Cu^I complexes formed linear species, $[Cu(OR)_2]^{1-}$, the complexes with bidentate pin^F required an additional ligand, PPh_3, to stabilize the coordination sphere in $[(R_3P)Cu(pin^F)_2]^{1-}$. When O_2 was added, the PPh_3 was oxidized and no longer bound to Cu, with the resulting $OPPh_3$ quantified at 88% by ^1H NMR, giving way for the reactive trinuclear core.[22] In that work,

the identity of phosphine was shown to affect oxidase catalysis by the intermediate trimer. The employment of Pcy_3, versus PPh_3, in the precatalyst was shown to double the turnover number (TON) of hydroquinone to benzoquinone, which phenomenon is not presently understood. Despite successfully synthesizing numerous homoleptic 3*d* fluorinated alkoxides, to date, no other related alkoxide complexes without Cu^{I} have been examined for O_2 reactivity. Additionally, these Cu^{I} complexes are both light and temperature sensitive and require low temperatures to form intermediates that can achieve intermolecular oxidation. A more stable precatalyst that could be activated under mild reaction conditions is desirable. While an electron rich Cu^{I} center allowed for the low coordination number around Cu, exploration of less electron rich 3*d* metals will require additional supporting ligand(s) for stabilization.

Phosphines are common ligands in inorganic chemistry, capable of acting as strong σ-donors and weak π-acceptors. These ligands are commonly used in cross-coupling catalysts, including Sonogashira, Negishi, Stille, and Suzuki cross-couplings.[24] In these Pd-catalyzed cross-coupling reactions, both the steric and electronic properties of phosphines were investigated to maximize catalytic efficiency. Bulky ligands were found to effect reactivity best, with ligand selection shown to influence chemoselectivity.[25] The benefit of a supporting ligand such as phosphine on a reduced metal center is that these ligands typically do not react, but instead just dissociate. A limited number of 3*d* complexes have been made with solely PPh_3 and O-donor ligands in the environment, with either Cu[22, 26-34] or Zn[35-37] as the metal center.

In expanding beyond Cu to earlier metals, metal centers with fewer *d* electrons might require greater numbers of ligands compared to the previously described $\{Cu(OR)_2\}^-$ complexes. This principle is likely to also be seen in the relative stabilities of any intermediates formed upon reaction with O_2. As previously shown in our Cu^{I} work, and the work of many others, Cu^{I} can be stabilized by two donors, and when exposed to O_2 under controlled conditions, can be oxidized to Cu^{II} or Cu^{III} in forming reactive intermediates with a minimum coordination number of three.[9-11, 20] Such $\{Cu_xO_y\}$ chemistry has been widely explored, particularly as potential biological

mimics of enzyme active sites, with nearly all N-donor ligands. Upon controlled reduction of O_2, Cu can form $\{Cu_xO_y\}$ cores including mononuclear $\{Cu^{III}(\eta^2\text{-}O_2)\}$ peroxo, $\{Cu^{II}(\eta^1\text{-}O_2)\}$ superoxo, and $\{Cu^{II}(\eta^2\text{-}O_2)\}$ superoxo, dinuclear bis-μ-oxo $\{Cu^{III}(\mu_2\text{-}O_2)\}$, $\{Cu^{II}(\mu\text{-}\eta^2\text{:}\eta^2\text{-}O_2)\}$ peroxo, and $\{Cu^{II}(\mu\text{-}\eta^1\text{:}\eta^1\text{-}O_2)\}$ peroxo, as well as a symmetric trinuclear core, $\{Cu_3(\mu_3\text{-}O)_2\}$. Our work marks the only fully O-donor $\{Cu_xO_y\}$ studies performed, as discussed above, resulting in the formation of $\{Cu_3(\mu_3{-}O)_2\}$ regardless of ligand coordination.[21-23]

As with Cu, $\{Fe_xO_y\}$ chemistry has also been widely studied with model complexes in order to understand enzyme structure and function.[3, 4, 38-41] Fe is commonly known to form numerous mono- and dinuclear $\{Fe_xO_y\}$ intermediates, including the mononuclear $\{Fe^{III}(\eta^2\text{-}O_2)\}$ peroxo and –superoxo species, as well as Fe^{IV} and Fe^{V}-oxo moieties.[42] Dinuclear cores include $\{Fe^{III}{}_2(\mu\text{-}\eta^1\text{:}\eta^1\text{-}O_2)\}$ peroxo, $\{Fe^{II}Fe^{III}(\mu\text{-}\eta^1\text{:}\eta^2\text{-}O_2)\}$ superoxo, as well as the oxo-containing $\{Fe^{IV}{}_2((\mu_2\text{-}O)_2\}$, and $\{Fe^{III}Fe^{IV}(\mu_2\text{-}O)_2\}$.[3, 4] Coordination numbers at Fe are typically five to six in the intermediates of non-heme Fe^{II} complex reactions with O_2.

Compared to Fe and Cu, Ni- and Co-based systems are far less utilized in biological O_2 metabolism and are therefore less well-studied in model complexes. In nature, Co can be found in certain extradiol catechol dioxygenases, and the mechanism of this enzyme differs in that substrate binding occurs before formation of a $\{Co_xO_y\}$ species at the active site.[43, 44] Nevertheless, non-biomimetic $\{Co_xO_y\}$ species have been prepared for C-H oxidation use. Less electron-rich, square-planar Co^{II} complexes in rigid ligand environments, such as that of a porphyrin, are known to form relatively stable $\{Co^{III}(\eta^1\text{-}O_2)\}$ superoxo species upon reaction with O_2, and these have been reviewed.[43, 45-47] More recently, more reactive $\{Co_xO_y\}$ species were reported, including $\{Co^{II}(\eta^2\text{-}O_2)\}$ superoxo and $\{Co^{III}(\eta^2\text{-}O_2)\}$ peroxo, as well as dimeric cores $\{Co^{III}{}_2(\mu_2\text{-}O)_2\}$ and $\{Co^{II}{}_2(\text{trans-}\mu\text{-}\eta^1\text{:}\eta^1\text{-}O_2)_2\}$, which has two bridging superoxide units. Coordination numbers at Co typically range between five and six.[43, 48 49] A particularly well known example of $\{Co_xO_y\}$ chemistry used the thioether borate scaffold, in which a Co^{I}

coordinated in a hydrotris(3-*tert*-butyl-5-methylpyrazolyl)borate ligand environment formed a crystallographically characterized mononuclear {$Co^{II}(\eta^2\text{-}O_2)$} superoxo species. However, when the steric bulk in the pyrazolyl 3 position is reduced from a *tert*-butyl substituent to an *iso*-propyl group, a temperature dependent equilibrium exists in CD_2Cl_2 between the monomeric side-on Co^{II}-superoxo, {$Co^{II}(\eta^2\text{-}O_2)$} and the dimeric Co^{II} μ-1,2-superoxo species, {$Co^{II}_2(\text{trans-}\mu\text{-}\eta^1\text{:}\eta^1\text{-}O_2)_2$} (Scheme 1, top).[50, 51]

In biological systems, Ni^{II}/Ni^{III} redox transformations are well-known, such as in superoxide dismutase (SOD) or [NiFe]-hydrogenase.[52, 53] This redox activity is proposed to be accessible due to the presence of radicals in the proximity of the active site.[54-56] Reactive {Ni_xO_y} cores include monomeric side-on {$Ni^{II}(\eta^2\text{-}O_2)$} superoxo and {$Ni^{III}(\eta^2\text{-}O_2)$} peroxo, as well as {$Ni^{III}_2(\mu_2\text{-}O)_2$} cores.[57-60] For such {Ni_xO_y} species, the coordination number is typically four or five. Similar to the {Co_xO_y} chemistry described above, a thioether tripodal borate ligand, phenyl[tris(alkylthiomethyl)]borate or {$PhB(CH_2SR)_3$}$^-$, was used to support a four-coordinate Ni center.[60] When the R group in the thioether is less the sterically hindering *tert*-butyl (^{t}Bu), the dimeric {$Ni^{III}_2(\mu_2\text{-}O)_2$} species is observed upon introduction of O_2 to the Ni^I initial complex, [{$PhB(CH_2SR)_3$}Ni(CO)]. However, when the particularly bulky 1-adamantyl group is employed, preventing dimerization, the mononickel(II)-superoxo core {$Ni^{II}(\eta^2\text{-}O_2)$} is formed (Scheme 1, bottom).

Based on the aforementioned use of PPh_3 as a protecting group,[22] we sought to expand upon this idea, by first using PPh_3 to prepare low-coordinate 3*d* fluorinated alkoxide complexes of the form {$(R_3P)_xM(OR)_y$}, and subsequently to examine whether these PR_3 ligands could be oxidatively removed by O_2 addition to form to reactive {M_xO_y} intermediates. Transition metals with bulky hydrogenated alkoxide ligands have been shown to perform oxo, nitrene, and carbene transfer and have recently been reviewed.[61] Herein, we discuss the synthesis and structural properties of 3*d* complexes with several new heteroleptic phosphine and fluorinated

alkoxide ligand environments, including PPh_3/fluorinated-alkoxide complexes with Fe, Co, and Ni metal centers. This work begins to explore the question of how many supporting ligands are required to stabilize {$M(OR)_2$}-containing 3*d* complexes to permit controlled O_2 reduction and C-H bond oxidation. In this new structural family, there are two phosphine groups and two O-donors. To evaluate the role of PPh_3 as a potential leaving group, these complexes were reacted with O_2 and studied for identification of intermediates and/or terminally oxidized species.

Experimental

Materials and methods

All complexes were prepared at room temperature in an MBraun purified N_2-filled drybox. Hexanes, CH_2Cl_2, THF (for synthesis), and Et_2O were dried in an alumina-based solvent purification system (SPS) under Ar(g) directly connected to the drybox and stored over molecular sieves. THF (for O_2 reactivity), toluene and dimethoxyethane (DME) were dried by refluxing over Na/benzophenone under an N_2 atmosphere, distilled, and stored over molecular sieves. NMR samples prepared under N_2 used $CDCl_3$, d_6-acetone, or CD_3CN, which were stored over sieves in the drybox. Alcohols HOC_4F_9 and H_2pin^F were obtained from Oakwood Chemicals and were dried over sieves and distilled, and stored over sieves in the drybox. KOC_4F_9 was prepared according to the previously reported method.[62] $Ni(CH_3CN)_4(OTf)_2$ was prepared according to the previously reported method.[63] PhSMe was dried over CaH_2, distilled, and stored over molecular sieves. Sodium 2,4-di-*tert*-butylphenolate (DBP) was synthesized by combining 2,4-di-*tert*-butylphenol and sodium hydride at low temperature. All other reagents were obtained commercially and used without further purification.

UV-vis data were collected with a Shimadzu UV-3600 spectrometer. NMR spectra were recorded on a Varian ^1H 500 MHz spectrometer at room temperature. Chemical shifts for ^1H and $^{13}C\{^1H\}$ were referenced to the residual protio solvent resonance. $CFCl_3$ was used as an external standard for ^{19}F NMR. Solution phase magnetic susceptibilities were determined via the

Evans method[64, 65] in CD_3CN or $CDCl_3$ with 1% Me_4Si as an internal standard and reported after appropriate diamagnetic corrections. For low temperature Evans method and ^{31}P NMR, data were acquired on a Bruker ^1H 400 MHz spectrometer at Bruker BioSpin (Billerica, Massachusetts). Elemental analyses were performed by Atlantic Microlabs, Inc. (Norcross, Georgia).

Preparation of complexes

*$[(Ph_3P)_2Fe(OC_4F_9)_2]$ (**1**)*

A portion of $FeCl_2$ (0.135 g, 1.067 mmol) was slurried in 10 mL of THF and TlOTf (0.755 g, 2.136 mmol) was added directly to the $FeCl_2$ mixture as a solid, upon which an immediate precipitation of presumed TlCl was observed. This mixture was left to stir overnight at RT, and then filtered over Celite to remove TlCl, leaving a colorless solution. Two equiv of PPh_3 (0.560 g, 2.135 mmol) were dissolved in 2 mL THF and subsequently added to the reaction, stirring for 20 min. An equimolar portion of KOC_4F_9 (0.585 g, 2.134 mmol) was prepared in 2 mL THF, and added to the reaction mixture. The colorless solution was allowed to stir for 1.5 h. The reaction mixture was then dried in vacuo, triturated twice with hexanes, and dissolved in Et_2O, which allowed filtration to remove presumed insoluble KOTf. The colorless solution was dried in vacuo to a white solid, and then triturated three times with hexanes to a pale blue/white solid. Recrystallization by layering Et_2O and hexanes at −30 °C afforded pale blue crystals suitable for X-ray analysis in a 29% yield (0.654 g). UV-vis (Et_2O) [λ_{max}, nm (ε, M^{-1} cm^{-1})] 261 (30500). μ_{eff} (Evans method, CD_3CN): 4.48(4) (avg. of 2). Anal. Calcd. for $C_{44}H_{30}F_{18}FeO_2P_2$ (solvent-free complex): C, 50.31; H, 2.88; F, 32.55. Found: C, 50.59; H, 2.94; F, 32.26.

*$[(Ph_3P)_2Co(OC_4F_9)_2]$ (**2**)*

Method 1: A portion of $(Ph_3P)_2CoCl_2$ (0.2033 g, 0.311 mmol) was dissolved in 15 mL THF, affording a blue solution and TlOTf (0.220 g, 0.622 mmol) was added as a solid, upon which an immediate color change to pink and the precipitation of presumed TlCl was observed. This mixture was allowed to stir overnight at RT and was then filtered over Celite to remove TlCl.

Two equiv of KOC_4F_9 (0.171 g, 0.624 mmol) were dissolved in minimal THF and added to the pink reaction, affording a deep purple solution. Upon stirring for 1 h, the reaction mixture was then dried in vacuo to a purple oil, and stirred in hexanes. The purple solution was filtered through a pipette to remove presumed insoluble KOTf, which was triturated with hexanes to a purple powder and recrystallized by layering Et_2O and hexanes at −30 °C. The remaining material was dissolved in Et_2O, filtered to remove presumed insoluble KOTf, triturated with hexanes to a purple powder, and recrystallized from by layering Et_2O and hexanes at −30 °C, and slow evaporation from hexanes. Collection of all recrystallizations resulted in purple crystals with a 21.4% yield (0.070 g). A publishable structure was not obtained, but molecular connectivity was confirmed. Because of low yield, an alternative synthesis was pursued.

Method 2: A portion of $CoCl_2$ (0.116 g, 0.893 mmol) was dissolved in 15 mL of THF, affording a blue solution, to which TlOTf (0.631 g, 1.785 mmol) was added directly as a solid, upon which an immediate color change to pink and precipitation of presumed TlCl was observed. This mixture was left to stir overnight at RT, and then filtered over Celite to remove TlCl, leaving a pink solution. Two equiv of PPh_3 (0.469 g, 1.787 mmol) was dissolved in 2 mL of THF and subsequently added to the reaction, stirring for 10 min. KOC_4F_9 (0.490 g, 1.785 mmol) was prepared in 2 mL THF, and added to the reaction mixture where an immediate color change to a deep purple was observed. Upon stirring for 1.5 h, the reaction mixture was then dried in vacuo, triturated once with hexanes, and dissolved in Et_2O, which allowed filtration to remove presumed insoluble KOTf. The purple solution was dried in vacuo to a deep purple solid, and then triturated three times with hexanes to a purple powder. The product was recrystallized by making a concentrated solution in Et_2O with a few drops of hexanes and then layering with hexanes at −30 °C afforded deep purple crystals with a 68% yield (0.642 g). UV-vis (Et_2O) [λ_{max}, nm (ε, M^{-1} cm^{-1})] 261(38000), 515 (118), 570 (160), 683 (161). μ_{eff} (Evans method, CD_3CN): 4.0(1) (avg. of 2). Anal. Calcd. for $C_{44}H_{30}CoF_{18}O_2P_2$ (solvent-free complex): C, 50.16; H, 2.87; F, 32.46. Found: C, 50.19; H, 2.94; F, 32.33.

*[(Ph$_3$P)$_2$Ni(OC$_4$F$_9$)$_2$] (**3**)*

Method 1: A portion of (Ph$_3$P)$_2$NiCl$_2$ (0.150 g, 0.229 mmol) was dissolved in 10 mL THF as a pale yellow solution. TlOTf (0.162 g, 0.459 mmol) was slurried in 5 mL THF and added to the Ni solution, upon which an immediate precipitation of presumed TlCl was observed. The solution was allowed to stir overnight at RT, and then filtered over Celite to remove TlCl, leaving a pale yellow solution. Two equiv of KOC$_4$F$_9$ (0.126 g, 0.460 mmol) was prepared in minimal THF and added to the Ni solution, which changed to dark purple. The solution was left to stir for 2 h, dried in vacuo and dissolved in Et$_2$O, which allowed filtration to remove presumed insoluble KOTf. The purple solution was dried in vacuo and triturated once with toluene and three times with hexanes to a green solid. Recrystallization by layering Et$_2$O and hexanes at −30 °C afforded dark purple crystals suitable for X-ray analysis. Crystals were embedded in green solid, which could be washed off with hexanes. Because of byproduct, an alternative synthesis was pursued.

Method 2: A portion of Ni(CH$_3$CN)$_4$(OTf) (0.203 g, 0.390 mmol) was dissolved in THF affording a yellow-green solution, to which two equiv of KOC$_4$F$_9$ (0.214 g, 0.781 mmol) in 2 mL THF was added to the Ni solution, which changed to dark purple. After stirring for 10 min, an equimolar portion of PPh$_3$ (0.204 g, 0.778 mmol) in 2 mL THF was added to the solution, after which the solution became a slightly darker purple. The solution was allowed to stir for 2 h, followed by concentration and trituration with Et$_2$O. The purple solid was then dissolved in Et$_2$O, which allowed filtration of presumed insoluble KOTf. The purple solution was dried in vacuo to a green-grey solid, and then triturated three times with hexanes. The product was doubly recrystallized by layering Et$_2$O and hexanes at −30 °C, affording dark purple crystals at a 45% yield (0.183 g). UV-vis (Et$_2$O) (λ_{max}, nm (ε, M^{-1} cm^{-1})): 261 (47000), 477 (60), 555 (67), 610 (61). μ_{eff} (Evans method, CD$_3$CN): 3.27(8) (avg. of 2). Anal. Calcd. for C$_{44}$H$_{30}$F$_{18}$NiO$_2$P$_2$ (solvent-free complex): C, 50.17; H, 2.87; F, 32.47. Found: C, 49.95; H, 3.07; F, 32.25.

*[(Ph$_3$P)$_2$Zn(OC$_4$F$_9$)$_2$] (**4**)*

A portion of ZnI_2 (0.163 g, 0.511 mmol) was slurried in 10 mL of THF and TlOTf (0.361 g, 1.021 mmol) was added directly to the $ZnCl_2$ mixture as a solid, upon which an immediate precipitation of presumed TlI was observed. This mixture was left to stir overnight at RT, and then filtered over Celite to remove TlI, leaving a slightly pale yellow solution. Two equiv of PPh_3 (0.268 g, 1.020 mmol) was dissolved in minimal THF and subsequently added to the reaction, stirring for 20 min. An equimolar portion of KOC_4F_9 (0.280 g, 1.020 mmol) was prepared in minimal THF, and added to the reaction mixture. The colorless solution was allowed to stir for 1.5 h. The reaction mixture was then dried in vacuo, triturated twice with hexanes, and dissolved in Et_2O, which allowed filtration of presumed insoluble KOTf. The colorless solution was dried in vacuo to a white solid, and then triturated twice with hexanes to a white powder. Recrystallization by layering Et_2O and hexanes at −30 °C afforded colorless crystals in an 83% yield (0.225 g). Crystals grown by layering CH_2Cl_2 and hexanes at −30 °C confirmed molecular connectivity. UV-vis (Et_2O) (λ_{max}, nm (ε, M^{-1} cm^{-1})): 261 (50000). ^{1}H NMR (500 MHz, CD_3CN), δ= 7.39 ppm (m, 3H, *o*, *p*-C_6H_5), 7.30 ppm (m, 2H, *m*-C_6H_5). ^{13}C NMR (125 MHz, CD_3CN), δ= 137.81 ppm (d, ^{1}J(C,P)= 8.75 Hz, *ipso*-C_6H_5), 134.47 (d, ^{2}J(C,P)= 18.75 Hz, *o*-C_6H_5), 130.00 (s, *p*-C_6H_5), 129.65 (d, ^{3}J(C,P)= 7.50 Hz, *m*-C_6H_5). ^{19}F NMR (470 MHz, CD_3CN), δ= −74.88 ppm (s, $OC(CF_3)_2$. Anal. Calcd. for $C_{44}H_{30}F_{18}O_2P_2Zn$ (solvent-free complex): C, 49.86; H, 2.85; F, 32.26. Found: C, 49.65; H, 2.93; F, 31.96.

*[(DME)Fe(OC_4F_9)$_2$] (**5**)*

A portion of $FeCl_2$ (0.139 g, 1.098 mmol) was slurried in 10 mL of THF and TlOTf (0.777 g, 2.198 mmol) was added directly to the $FeCl_2$ mixture as a solid, upon which an immediate precipitation of presumed TlCl was observed. This mixture was left to stir overnight at RT, and then filtered over Celite to remove TlCl, leaving a colorless solution. Sub-stoichiometric DME (0.0868 g, 0.963 mmol) was directly added and allowed to stir for 5 min. Two equiv of KOC_4F_9 (0.602 g, 2.196 mmol) was then prepared in 2 mL THF and added to the reaction mixture. The colorless solution was allowed to stir for 45 min. The reaction mixture was then dried in vacuo,

triturated once with hexanes, and dissolved in Et_2O, which allowed filtration of presumed insoluble KOTf. The brown tinted solution was dried in vacuo to a pale peach oil, and then triturated twice with hexanes to an off-white/beige solid. Recrystallization by layering Et_2O and hexanes at −30 °C afforded beige multi-crystalline material in a 35% yield (0.233 g). UV-vis (Et_2O) (λ_{max}, nm (ε, M^{-1} cm^{-1})): 231 (232), 288 (86, shoulder). μ_{eff} (Evans method, CD_3CN): 4.67(7) (avg. of 2). Anal. Calcd. for $C_{12}H_{10}F_{18}FeO_4$ (solvent-free complex): C, 23.40; H, 1.64; F, 55.51. Found: C, 23.76; H, 1.92; F, 48.50. Fluorine analysis is likely low because of incomplete combustion of F atoms.

*[$(Ph_3PO)_2Fe(OC_4F_9)_2$] (**6**)*

A portion of $FeCl_2$ (0.134 g, 1.057 mmol) was slurried in 10 mL of THF and TlOTf (0.747 g, 2.114 mmol) was added directly to the $FeCl_2$ mixture as a solid, upon which an immediate precipitation of presumed TlCl was observed. This white cloudy mixture was left to stir overnight at RT, and then filtered over Celite, leaving a colorless solution. Two equiv of $OPPh_3$ (0.588 g, 2.113 mmol) was dissolved in 5 mL THF and subsequently added to the reaction, stirring for 10 min. An equimolar portion of KOC_4F_9 (0.580 g, 2.116 mmol) was prepared in 2 mL THF and added to the reaction mixture. The slightly cloudy solution was allowed to stir for 1.5 h. The reaction mixture was then dried in vacuo to a white solid, triturated three times with hexanes, and dissolved in Et_2O, which allowed filtration of presumed insoluble KOTf. The colorless solution was dried in vacuo to a white solid, and then triturated three times with hexanes to a white powder. Recrystallization by layering Et_2O and hexanes at −30 °C afforded colorless crystals suitable for X-ray analysis in a 70% yield (0.795 g). UV-vis (Et_2O) (λ_{max}, nm (ε, M^{-1} cm^{-1})): 264 (14800), 271 (13100, shoulder), 325 (4200, shoulder). μ_{eff} (Evans method, CD_3CN): 4.2(1) (avg. of 2). Anal. Calcd. for $C_{44}H_{30}F_{18}FeO_4P_2$ (solvent-free complex): C, 48.82; H, 2.79; F, 31.59. Found: C, 48.64; H, 2.73; F, 31.57.

*[$(Ph_3PO)_2Ni(OC_4F_9)_2$] (**7**)*

A portion of $Ni(CH_3CN)_4(OTf)$ (0.402 g, 0.772 mmol) was dissolved in THF affording a yellow-green solution, to which two equiv of $OPPh_3$ (0.365 g, 1.311 mmol) in 2 mL THF was added to the reaction, stirring for 10 min. An equimolar portion of KOC_4F_9 (0.423 g, 1.543 mmol) was prepared in 2 mL THF, and added to the reaction mixture upon which an immediate color change to deep purple was observed. Upon stirring for 1 h, the reaction mixture was dried in vacuo to a purple-blue solid, triturated once with hexanes, and dissolved in Et_2O, which allowed filtration of presumed insoluble KOTf. The solution was dried in vacuo, and then triturated three times with hexanes to a purple-blue powder. Recrystallization by layering CH_2Cl_2 and hexanes at −30 °C afforded blue crystals with a 50% yield (0.357 g). Crystals suitable for X-ray analysis were obtained by layering Et_2O and hexanes at −30 °C. UV-vis (Et_2O) (λ_{max}, nm (ε, M^{-1} cm^{-1})): 224 (166000), 260sh (5400), 265 (5860), 272 (4560, shoulder), 314 (540, shoulder), 480 (38), 572 (64), 620 (50, shoulder). μ_{eff} (Evans method, CD_3CN): 3.07(8) (avg. of 2). Anal. Calcd. for $C_{44}H_{30}F_{18}NiO_4P_2$ (solvent-free complex): C, 48.69; H, 2.79; F, 31.51. Found: C, 48.39; H, 2.78; F, 31.25.

*$[(Ph_3P)_2Co(pin^F)]$ (**8**)*

A portion of $[(Ph_3P)_2Co(OC_4F_9)_2]$, **2**, (0.189 g, 0.179 mmol) was dissolved in 10 mL Et_2O, affording a deep purple solution. An equimolar portion of H_2pin^F (0.0605, 0.181 mmol) in 2 mL Et_2O was added dropwise over 1 min, and an immediate color change to deep blue was observed. The solution was allowed to stir overnight, and was then dried in vacuo to a blue oil. Trituration three times with hexanes led to a blue powder, which was recrystallized by layering Et_2O and hexanes at −30 °C. Deep blue crystals suitable for X-ray analysis were collected in a 75% yield (0.122 g). Crystals suitable for X-ray analysis were obtained by layering CH_2Cl_2 and hexanes at −30 °C. UV-vis (CH_2Cl_2) (λ_{max}, nm (ε, M^{-1} cm^{-1})): 259 (46100), 585 (110), 621 (113). μ_{eff} (Evans method, $CDCl_3$): 4.2(3) (avg. of 2). Anal. Calcd. for $C_{42}H_{30}CoF_{12}O_2P_2$ (solvent-free complex): C, 55.10; H, 3.30; F, 24.90. Found: C, 55.08; H, 3.40; F, 24.95.

*$[(Ph_3P)_2Ni(pin^F)]$ (**9**)*

Method 1: A portion of $(Ph_3P)_2NiCl_2$ (0.149 g, 0.228 mmol) was dissolved in 10 mL THF as a pale yellow solution and TlOTf (0.163 g, 0.460 mmol) was suspended in minimal THF and added, upon which an immediate precipitation of presumed TlCl was observed. The solution was allowed to stir overnight at RT, and then filtered over Celite to remove TlCl, leaving a pale yellow solution. In a separate vial, two equiv of NEt_3 (0.0447 g, 0.442 mmol) was added to one equiv of H_2pin^F (0.0766 g, 0.229 mmol) in 5 mL THF and allowed to stir for 20 min. The solution was then added to the Ni solution, upon which an immediate color change to dark orange was observed. This reaction was allowed to stir for 2 h, dried in vacuo, and triturated with toluene and hexanes to an orange solid. Orange crystals suitable for X-ray analysis were grown by layering THF and hexanes at −30 °C. Due to inseparable N−based impurities determined by elemental analysis, an alternate synthesis was pursued. Anal. Calcd. for $C_{42}H_{30}F_{12}NiO_2P_2$ (solvent-free complex): C, 55.11; H, 3.30; F, 24.91. Found: C. 48.41; H, 3.44; N, 0.56; F, 29.40.

Method 2: A portion of $[(Ph_3P)_2Ni(OC_4F_9)_2]$, **3**, (0.0664 g, 0.0630 mmol) was dissolved in 10 mL THF, affording a purple solution. An equimolar portion of H_2pin^F (0.0220 g, 0.0659 mmol) in 1 mL THF was added dropwise over 1 min, upon which an immediate color change to orange was observed. The solution was allowed to stir overnight and was then dried in vacuo to an orange solid and triturated twice with hexanes to an orange powder. Recrystallization by layering THF and hexanes at −30 °C resulted in orange crystals in a 59% yield (0.0342 g). UV-vis (Et_2O) (λ_{max}, nm (ε, M^{-1} cm^{-1})): 262 (38500), 470 (272). ^{1}H NMR (500 MHz, $CDCl_3$), δ= 7.54 ppm (m, 2H, *o*-C_6H_5), 7.34 ppm (m, 1H, *p*-C_6H_5), 7.19 ppm (m, 2H, *m*-C_6H_5). ^{13}C NMR (125 MHz, $CDCl_3$), δ= 134.11 ppm (t, ^{1}J(C,P)= 5.00 Hz, *ipso*-C_6H_5), 130.30 ppm (s, *o*-C_6H_5), 128.52 ppm (t, ^{4}J(C,P)= 23.75 Hz, *p*-C_6H_5), 127.92 (t, ^{3}J(C,P)= 5.00 Hz, *m*-C_6H_5). ^{19}F NMR (470 MHz, $CDCl_3$), δ= −70.79 ppm (s, $OC(CF_3)_2$). Anal. Calcd. for $C_{42}H_{30}F_{12}NiO_2P_2$ (solvent-free complex): C, 55.11; H, 3.30; F, 24.91. Found: C, 55.38; H, 3.36; F, 25.12.

*$[(Ph_3P)_2Zn(pin^F)]$ (**10**)*

A portion of $[(Ph_3P)_2Zn(OC_4F_9)_2]$, **4**, (0.245 g, 0.232 mmol) was dissolved in 10 mL Et_2O, affording a colorless solution. An equimolar portion of H_2pin^F (0.0780 g, 0.233 mmol) in 3 mL Et_2O was added dropwise over 1 min. The colorless solution was allowed to stir overnight, and was then dried in vacuo to a white solid and triturated with hexanes to a white powder. Recrystallization by layering CH_2Cl_2 and hexanes at −30 °C resulted in colorless crystals suitable for X-ray analysis in a 68% yield (0.145 g). UV-vis (Et_2O) (λ_{max}, nm (ε, M^{-1} cm^{-1})): 262 (46200). ^{1}H NMR (CD_3CN, 500 MHz), δ= 7.38 ppm (m, 3H, *o*,*p*-C_6H_5), 7.30 ppm (m, 2H, *m*-C_6H_5). ^{13}C NMR (CD_3CN, 125 MHz), δ= 138.09 ppm (d, $^1J(C,P)$= 11.25 Hz, *ipso*-C_6H_5), 134.47 (d, $^2J(C,P)$= 25.00 Hz, *o*-C_6H_5), 129.93 (s, *p*-C_6H_5), 129.64 (d, $^3J(C,P)$= 7.50 Hz, *m*-C_6H_5). ^{19}F NMR (CD_3CN, 470 MHz), δ= −70.72 ppm (s, $OC(CF_3)_2$). Anal. Calcd. for $C_{42}H_{30}F_{12}O_2P_2Zn$ (solvent-free complex): C, 54.71; H, 3.28; F, 24.73. Found: C, 53.80, H, 3.26; F, 24.17. EA consistent with ¼ molecule of CH_2Cl_2, which is present in the structure.

*$[Co_2(pin^F)_2(THF)_4]$ (**11**)*

A portion of $[(Ph_3P)_2Co(OC_4F_9)_2]$, **2**, (0.125 g, 0.119 mmol) was dissolved in 10 mL THF, affording a deep purple solution. An equimolar portion of H_2pin^F (0.040 g, 0.120 mmol) in 2 mL THF was added dropwise over 1 min, upon which an immediate color change to magenta was observed. The solution was allowed to stir overnight, and was then dried in vacuo to a purple-blue solid and triturated two times with hexanes to a purple-blue powder. Recrystallization by layering THF and hexanes at −30 °C resulted in purple crystals in a 31.7% yield (0.020 g). A publishable structure was not obtained, but structural connectivity was confirmed (Figure A.4). UV-vis (THF) (λ_{max}, nm (ε, M^{-1} cm^{-1})): 260 (2090), 451 (44), 556 (54), 853 (11). μ_{eff} (Evans method, $CDCl_3$): 3.071(5) (per Co; avg. of 2). Anal. Calcd. for $C_{28}H_{32}Co_2F_{24}O_8$ (solvent-free complex): C, 31.42; H, 3.01; F, 42.60. Found: C, 31.49; H, 3.07; F, 42.41.

*$[Zn_2(pin^F)_2(THF)_2]$ (**12**)*

A portion of $[(Ph_3P)_2Zn(OC_4F_9)_2]$, **4**, (0.0438 g, 0.0414 mmol) was dissolved in 5 mL of THF, affording a colorless solution. An equimolar portion of H_2pin^F was dissolved in 1 mL of THF and

added dropwise over 1 min to the Zn solution. The reaction was allowed to stir overnight, and was then dried in vacuo to a white solid, followed by two triturations with hexanes. The resulting white powder was recrystallized by layering THF and hexanes at −30 °C, affording colorless crystals in a 13% yield (0.0050 g). Because of low yield, this species was neither pursued nor characterized further. Anal. Calcd. for $C_{20}H_{16}F_{24}O_6Zn_2$ (solvent-free complex): C, 25.58; H, 1.72. Found: C, 25.37; H, 1.99.

*[$(F_9C_4O)_2(Ph_3PO)Fe(\mu$-O)Fe$(OPPh_3)(OC_4F_9)_2$] (**13**)*

A portion of [$(Ph_3P)_2Fe(OC_4F_9)_2$], **1**, (0.176 g, 0.167 mmol) was dissolved in 3 mL THF, affording a colorless solution. This solution was sealed in a Schlenk flask equipped with a septum, brought to the Schlenk line, and cooled to −78 °C in a dry ice/acetone bath. O_2 added directly via balloon and syringe for 5 min, during which the solution changed to a light orange. The solution was allowed to stir at low temperature for an additional 30 min, and then was warmed to RT, affording an orange solution. The solution was dried in vacuo to an orange oil, brought back into the drybox, stirred over hexanes and then triturated to afford a yellow-orange solid. The solid was dissolved in Et_2O, and dark orange solids were filtered off. Orange crystals suitable for X-ray analysis were grown from two recrystallizations layering Et_2O and hexanes at −30 °C, with an overall yield of 23% (0.0315 g). UV-vis (Et_2O) (λ_{max}, nm (ε, M^{-1} cm^{-1})): 222 (1440000) 261 (42700), 340 (7500, shoulder). μ_{eff} (Evans method, CD_3CN): 2.0(1) (per Fe, avg. of 2). Anal. Calcd. for $C_{52}H_{30}F_{36}Fe_2O_7P_2$ (solvent-free complex): C, 38.45; H, 1.86; F, 42.10. Found: C, 38.16; H, 2.00; F, 41.83.

X-ray crystallography

All data were collected on a Bruker Ultra mini-rotating anode (Mo Kα) diffractometer with micro-focus optics and an ApexII CCD detector at 100K, except for **6**, which was run at 150K due to crystal disintegration at 100K (likely the result of a phase transformation). Standard procedures were used for the integration and scaling of the data using software packages (SAINT and

APEXIII, Bruker Corp., Madison, WI). Subsequent refinement and treatment of disorder used the programs contained in the Olex2 software.[66]

Low temperature UV-vis spectroscopy

The UV-vis was cooled to the desired temperature and a baseline was taken with dried and distilled solvent. Under inert atmosphere, complexes were dissolved in desired solvent, and transferred to a Schlenk cuvette equipped with a septum. The complex was loaded into the instrument, and O_2 was introduced via balloon equipped with needle and syringe.

Low temperature NMR

For $[(Ph_3P)_2Ni(OC_4F_9)_2]$ (**3**), Evans method experiments, 2 solutions (8.1 mg and 16.1 mg) were prepared in d_8-THF with hexamethyldisiloxane (HMDSO) as an internal standard (5 drops per 3 g). Phosphorus and proton data were acquired on a Bruker Avance NEO 400 MHz spectrometer, at Bruker BioSpin (Billerica, Massachusetts), with a resonance frequency of 400.01 MHz for protons and 161.93 MHz for phosphorus. For the 8.1 mg sample, spectra were acquired at 293 K, 193 K and 273 K. For the proton spectra 64 transients with a spectral width of 19.5 ppm and a pulse corresponding to a 30 degree flip angle were used. Total recycle time between transients was 6.2 seconds. The phosphorus spectra were acquired with 64 transients with a total recycle time of 2.1 seconds, a 30 degree flip angle and a 406 ppm spectra width. For the 16.1 mg sample, proton and phosphorus spectra were acquired at 293 K and 193 K. Proton and phosphorus conditions were identical the sample 8.1 mg sample. All phosphorus spectra were acquired with proton decoupling.

*Reaction of **5-O₂** with H_2Q*

The evaluation of substrates was based on similar reactions investigated with related Cu-O_2 chemistry. In the drybox, Fe^{II} complexes were dissolved in THF in a Schlenk flask and transferred to the Schlenk line under N_2 atmosphere. The solution was cooled to −78 °C using a dry ice/acetone bath, and then O_2 bubbled into the solution from a balloon fitted with a syringe and needle. Upon introduction of O_2, the solution immediately turned pale yellow. After 1 min,

the O_2 source was removed and the solution was allowed to stir for 2 min. In the drybox, 10 equiv of H_2Q were measured out and dissolved in 1.0 mL THF, and sealed in a vial fitted with a septum. The H_2Q was then syringed and the solution immediately turned dark and cloudy. The solution was allowed to stir at low temperature for 30 min where no further changes were observed. The low temperature bath was removed, and the solution was allowed to stir for 1 h, settling as a clear solution with dark precipitate. The solution was quenched with 3 mL 0.5 M HCl. The pale yellow solution was partially concentrated to remove THF, followed by three extractions into Et_2O. The organic layer was concentrated to a yellow oil, which was dissolved in d_6-acetone with DMSO as an internal standard. The starting material and products were quantified by ^{1}H NMR. See Tables 4 and A.3 for calculation of H_2Q and BQ yields.

*Reaction of **5-O₂** with PhSMe*

The reaction flask was prepared and O_2 introduced as described in the above preparation. In the drybox, a 0.254 M stock solution of PhSMe in THF was prepared. 5 equiv PhSMe was dissolved in THF, sealed in a vial fitted with a septum and brought out of the drybox. After the flask stirred for 2 min following O_2 addition, PhSMe was syringed in, and the solution remained a pale yellow. The reaction was allowed to stir 30 min at low temperature, and then the bath was removed and the solution allowed to stir an additional 30 min. The yellow-orange solution was quenched with 3 mL 0.5 M HCl. The solution was partially concentrated to remove THF, followed by three extractions into CH_2Cl_2. The organic layer was concentrated to a yellow oil, which was dissolved in d_6-acetone with DMSO as an internal standard. The starting material and products were quantified by ^{1}H NMR. See Table 4 for PhSMe and methyl phenyl sulfoxide yields. Due to the liquid property of PhSMe, some starting material was likely lost during work-up, lowering the recovered material.

*Reaction of **6-O₂** with H_2Q*

The evaluation of substrates was based on similar reactions investigated with related Cu-O_2 chemistry. In the drybox, Fe^{II} complexes were dissolved in THF in a Schlenk flask and

transferred to the Schlenk line under N_2 atmosphere. The solution was cooled to −78 °C using a dry ice/acetone bath, and then O_2 bubbled into the solution from a balloon fitted with a syringe and needle. Upon introduction of O_2, the solution immediately turned bright yellow. After 1 min, the O_2 source was removed and the solution was allowed to stir for 5 min. In the drybox, 10 equiv of H_2Q were measured out and dissolved in 1.0 mL THF, and sealed in a vial fitted with a septum. The H_2Q was then syringed and an immediate color change to darker yellow occurred. The solution was allowed to stir at low temperature for 30 min, with the solution a pale brown color. The low temperature bath was removed, and the solution was allowed to stir for 1 h. The brown solution was quenched with 3 mL 0.5 M HCl. The solution was partially concentrated to remove THF, followed by three extractions into Et_2O. The organic layer was concentrated to a yellow oil, which was dissolved in d_6-acetone with DMSO as an internal standard. The starting material and products were quantified by ^{1}H NMR. See Tables 4 and A.3 for calculation of H_2Q and BQ yields.

*Reaction of **6-O₂** with PhSMe*

The reaction flask was prepared and O_2 introduced as described in the above preparation. In the drybox, a 0.254 M stock solution of PhSMe in THF was prepared. 5 equiv PhSMe were dissolved in THF, sealed in a vial fitted with a septum and brought out of the drybox. After the flask stirred for 5 min following O_2 addition, PhSMe was syringed in, and the solution remained pale yellow. The reaction was allowed to stir 30 min at low temperature, and then the bath was removed, and the solution was allowed to stir an additional 30 min. The yellow-orange solution was quenched with 3 mL 0.5 M HCl. The solution was partially concentrated to remove THF, followed by three extractions into CH_2Cl_2. The organic layer was concentrated to a yellow oil, which was dissolved in d_6-acetone with DMSO as an internal standard. The starting material and products were quantified by ^{1}H NMR. See Table 4 for PhSMe and methyl phenyl sulfoxide yields. Due to the liquid property of PhSMe, some starting material was likely lost during work-up, lowering the recovered material.

Results and discussion

Synthesis

A series of mixed fluorinated alkoxide and phosphine complexes was synthesized, with the general compositions $[(Ph_3P)_2M(OC_4F_9)_2]$ and $[(Ph_3P)_2M(pin^F)]$ (Scheme 2). These fluorinated alkoxide complexes feature either two monodentate OC_4F_9 ligands or one bidentate perfluoropinacolate (pin^F) ligand. Complexes of the form $[(Ph_3P)_2M(OC_4F_9)_2]$ were synthesized from the reaction of a metal triflate salt with two equivalents of PPh_3 and two equivalents of KOC_4F_9 (Scheme 2). To prepare $[(Ph_3P)_2Fe(OC_4F_9)_2]$ (**1**), $[(Ph_3P)_2Co(OC_4F_9)_2]$ (**2**), and $[(Ph_3P)_2Zn(OC_4F_9)_2]$ (**4**), a metal triflate was formed *in situ* from MX_2 and TlOTf in THF. Two equivalents of PPh_3 were added, followed by two equivalents of KOC_4F_9. The final products were separated from KOTf and recrystallized from Et_2O and hexanes, affording crystalline product in good yield. Compound **1** was isolated as pale blue crystals, **2** crystals were deep purple, and **4** was colorless.

Because NiX_2 (X = Cl, Br, I) did not react with TlOTf in THF, an alternative synthesis was devised for $[(Ph_3P)_2Ni(OC_4F_9)_2]$ (**3**). The known[63] $Ni(CH_3CN)_4(OTf)_2$ was dissolved in THF, and a color change from pale yellow to purple was observed when KOC_4F_9 was added, followed by PPh_3. Recrystallization of the final product from CH_2Cl_2 and hexanes afforded dark purple crystals in modest yield. The versatility of this synthesis was shown by substitution of PPh_3 to make derivative complexes. The phosphine-free $[(DME)Fe(OC_4F_9)_2]$ (**5**) was synthesized by the same route as **1**, and $[(Ph_3PO)_2Fe(OC_4F_9)_2]$ (**6**) was prepared with the two equivalents of $OPPh_3$. Similarly, $[(Ph_3PO)_2Ni(OC_4F_9)_2]$ (**7**) followed the same synthesis as **3**, with the exception of sub-stoichiometric $OPPh_3$ (1.7 equivalents). Stoichiometric addition of $OPPh_3$ to the reaction resulted in excess $OPPh_3$ in the product, which co-crystallized with **7** and was unable to be isolated due to similar solubility.

Following the synthetic pathway for **1**-**7**, syntheses of the perhydro [$(Ph_3P)_2Co(OC_4H_9)_2$] and [$(Ph_3P)_2Ni(OC_4H_9)_2$] were also attempted. In both cases, addition of KOtBu resulted in formation of insoluble purple solids that precipitated from solution. Due to the relatively high basicity of this alkoxide (pK_a of HOC_4H_9 (19.2) vs HOC_4F_9 (5.4))[67], the syntheses likely formed bridging oligomeric species.[68]

Addition of the pin^F ligand was most effective via alcoholysis of [$(Ph_3P)_2M(OC_4F_9)_2$] (M= Co (**2**), Ni (**3**), Zn (**4**)) with H_2pin^F (Scheme 2), to yield [$(Ph_3P)_2M(pin^F)$] (M= Co (**8**), Ni (**9**), Zn (**10**)). The reaction to form **9** was performed in THF, resulting in a change from purple to orange when H_2pin^F was added. For syntheses of **8** and **10**, the solvent influenced the final product of the alcoholysis reaction, and the reaction must be performed in Et_2O to attain the desired product. When H_2pin^F was added to **2** in THF, however, a color change to purple-pink was observed. After stirring overnight, the solution was concentrated and triturated with hexanes, and the purple-blue solid was then recrystallized by layering a THF solution with hexanes. The resulting purple crystals were determined to be dinuclear $Co_2(pin^F)_2(THF)_4$ (**11**), in which PPh_3 was displaced by THF. Notably, **11** is the first complex that contains bridging pin^F ligands. A similar phenomenon occurred when H_2pin^F was added to **4**, with the final product being $Zn_2(pin^F)_2(THF)_2$ (**12**), as determined by elemental analysis. Efforts to obtain the corresponding Fe complex with pin^F were made, via combination of **1** and stoichiometric H_2pin^F which led to a pale green solution. However, a stable product was unable to be crystallized, possibly due to displacement of PPh_3, leading to intractable mixtures.

Structural characterization

As discussed, PPh_3 is a widely used ligand in inorganic chemistry. Thousands of complexes have been synthesized that incorporate both a phosphine group and an O-donor source. Similarly, based on a search of the Cambridge Structural Database, over 900 complexes have at least one phosphine with at least one alkoxide on a transition metal center, showing how

widely phosphines have been used in inorganic synthesis. Restricting further, there are still over 250 complexes that have at least one PPh_3 with at least one alkoxide on a transition metal center. A majority of these complexes have either 4*d* or 5*d* metal centers, and have other ligands in addition to the alkoxide and phosphine, including halides, carbenes, and N-donor ligands.

Far fewer 3*d* metal centers have both at least one PPh_3 and one alkoxide as ligands, with 30 complexes structurally characterized to date. When these complexes were limited to solely PPh_3 and O-donor ligand environment, only 16 complexes were identified, all with either Cu[22, 26-34] or Zn[35-37] as the metal center. As Cu and Zn are more electron rich, this property may have led to greater complex stability, considering the size difference between a P atom and a 3*d* metal center. These complexes are the first Fe, Co and Ni alkoxides incorporating PPh_3 ligands to be reported.Single-crystal X-ray diffraction data were collected for $[(Ph_3P)_2M(OC_4F_9)_2]$ (M = Fe, **1,** and Ni, **3**) $[(Ph_3PO)_2M(OC_4F_9)_2]$ (M = Fe, **6** and Ni, **7**) and $[(Ph_3P)_2M(pin^F)]$ (M= Co, **8**, Ni, **9**, and Zn, **10)**. Selected angles and distances for these complexes are collected in Table 1, and τ_4 values (as well as magnetic data) are listed in Table 2. Full crystallographic data collection parameters are listed in Tables A.1 (OC_4F_9 complexes) and A.2 (pin^F complexes).

Table 1. Selected bond distances (Å) and angles (°) for $[L_2M(OR)_2]$ complexes.

Compound	Bond	Distance	Atoms	Angle
1	Fe−O(1)	1.898(2)	O(1)−Fe−O(2)	138.70(11)
	Fe−O(2)	1.880(2)	O(1)−Fe−P(1)	102.11(7)
	Fe−P(1)	2.4856(9)	O(1)−Fe−P(2)	99.73(8)
	Fe−P(2)	2.5092(9)	O(2)−Fe−P(1)	105.86(9)
			O(2)−Fe−P(2)	100.64(8)
			P(1)−Fe−P(2)	106.61(3)
3	Ni−O(1)	1.9185(19)	O(1)−Ni−O(2)	128.4(3)
	Ni−O(2)	1.907(6)	O(1)−Ni−P(1)	93.23(6)
	Ni−P(1)	2.3934(7)	O(1)−Ni−P(2)	105.88(7)
	Ni−P(2)	2.3580(8)	O(2)−Ni−P(1)	105.3(4)
			O(2)−Ni−P(2)	113.3(5)
			P(1)−Ni−P(2)	107.28(3)
6	Fe−O(1)	1.995(3)	O(1)−Fe−O(2)	94.08(11)
	Fe−O(2)	2.057(3)	O(1)−Fe−O(3)	102.80(12)

	Fe−O(3)	1.959(3)	O(1)−Fe−O(4)	127.44(13)
	Fe−O(4)	1.916(3)	O(2)−Fe−O(3)	106.46(11)
			O(2)−Fe−O(4)	99.91(12)
			O(3)−Fe−O(4)	120.63(12)
7	Ni−O(1)	1.9556(14)	O(1)−Ni−O(2)	101.93(6)
	Ni−O(2)	1.9700(14)	O(1)−Ni−O(3)	107.34(6)
	Ni−O(3)	1.9084(15)	O(1)−Ni−O(4)	93.54(6)
	Ni−O(4)	1.9071(14)	O(2)−Ni−O(3)	93.04(6)
			O(2)−Ni−O(4)	103.29(6)
			O(3)−Ni−O(4)	150.28(6)
8	Co−O(1)	1.9185(11)	O(1)−Co−O(2)	85.96(5)
	Co−O(2)	1.9140(11)	O(1)−Co−P(1)	124.84(4)
	Co−P(1)	2.3926(5)	O(1)−Co−P(2)	107.17(4)
	Co−P(2)	2.4256(5)	O(2)−Co−P(1)	108.28(4)
	C(2)−C(5)	1.647(2)	O(2)−Co−P(2)	124.76(4)
			P(1)−Co−P(2)	106.528(16)
9	Ni−O(1)	1.8698(16)	O(1)−Ni−O(2)	86.77(5)
	Ni−O(2)	1.8447(16)	O(1)−Ni−P(1)	83.84(5)
	Ni−P(1)	2.1956(7)	O(1)−Ni−P(2)	175.72(5)
	Ni−P(2)	2.1793(7)	O(2)−Ni−P(1)	170.22(5)
	C(1)-C(2)	1.617(4)	O(2)−Ni−P(2)	89.09(5)
			P(1)−Ni−P(2)	100.24(3)
10	Zn−O(1)	1.944(3)	O(1)−Zn−O(2)	86.90(12)
	Zn−O(2)	1.936(3)	O(1)−Zn−P(1)	108.21(9)
	Zn−P(1)	2.4109(11)	O(1)−Zn−P(2)	121.10(10)
	Zn−P(2)	2.4225(11)	O(2)−Zn−P(1)	122.04(9)
	C(1)-C(4)	1.672(6)	O(2)−Zn−P(2)	109.73(9)
			P(1)−Zn−P(2)	108.45(4)

The four-coordinate $[(Ph_3P)_2M(OC_4F_9)_2]$ complexes **1** (M = Fe) and **3** (Ni) are pseudo-tetrahedral as shown by τ_4 values of 0.81 and 0.83 (Table 2). Compound **1** has two nearly identical Fe−O distances averaging 1.889(9) Å. There is only one other complex with a $Fe-OC_4F_9$ bond, $\{K(18C6)[Fe(OC_4F_9)_3]\}$, which has slightly longer $Fe-OC_4F_9$ distances ranging from to 1.9660 Å to 1.9740 Å.[62] The Fe−P distances in **1** range from 2.4856(9) Å to 2.5092(9) Å and are noticeably longer than the average $Fe-PPh_3$ distance in the CSD of 2.26(7) Å. As expected, the M−O distances are shorter than M−P distances due to the anionic nature of the OC_4F_9 ligand as well as the larger size of P atom. As seen in Table 1 and in the left-hand ORTEP in Figure 1,

there is considerable distortion in the angles around the Fe center from 109.5°, as the largest angle of 138.70(11)°, O(1)−Fe−O(2), is likely due to interligand repulsion by CF_3 groups with both phosphines and alkoxides.

The structure of **3** is also pseudo-tetrahedral and similar to **1**, the angle with the greatest degree of distortion in **3** is that of O(1)−Ni−O(2) at 128.4(3)°. The Ni−P distances in **3** are unexceptional, ranging from 2.3934(7) Å to 2.3580(8) Å, again longer than the average Ni−PPh_3 distance of 2.20(5) Å. Only the related complex {K((18C6)}K[Ni(OC_4F_9)$_4$] also has Ni−OC_4F_9 bonds, with distances ranging from 1.863 Å to 1.973 Å, comparable to those in **3**.[69]

Due to rotational disorder in the CF_3 groups, only molecular connectivity was confirmed for **2** (Co) and **4** (Zn) (Figure A.1). A structure of [(Ph_3P)$_2$Zn(OC_4F_9)$_2$], **4**, was previously deposited into the CSD.[35] This structure is highly similar to **1** and **3**, as average Zn−O/P distances are both within 0.1 Å of those for the aforementioned complexes. Ligand angles around Zn are also similar, from 99.4(1)° to 119.9(2)°, and τ_4 is 0.88, again indicating a pseudo-tetrahedral geometry.

For the less sterically hindered [(Ph_3PO)$_2$Fe(OC_4F_9)$_2$], **6**, the τ_4 of 0.79 again indicates pseudo-tetrahedral geometry (Figure 1, right-hand side). Compared to **1**, the angle between OC_4F_9 groups at the Fe center decreases in **6** to 120.63(12)° due the additional O−P bond which further removes the phenyl bulk from the metal center. The largest angle at the Fe center of **6,** 127.44(13)°**,** is between one $OPPh_3$ group and one OC_4F_9. The Fe−OC_4F_9 distances, averaging 1.938 Å, are slightly longer than in **1**, and the Fe−$OPPh_3$ distances range from 1.995(3) Å to 2.057(3) Å, consistent with the four other complexes reported,[70-73] ranging from 1.982 Å to 2.116 Å.

Complex **7**, [(Ph_3PO)$_2$Ni(OC_4F_9)$_2$], has a τ_4 value 0.74, indicating a more distorted tetrahedron, one molecule of which is shown in Figure 2, compared to the τ_4 value of **6** (0.79), and consistent with a smaller atomic radius of Ni. As in **1** and **3**, the largest angle at the Ni center of 150.28(6)°

is between the OC_4F_9 groups. Significantly, the O(3)−Ni−O(4) angle in **7** is 21.88° more than in **3**, consistent with the Ni-containing complex having more structural distortion. The Ni−OC_4F_9 distances are nearly identical to those in **3** and are also comparable to those in the aforementioned {K(18C6)}K[Ni(OC_4F_9)$_4$].[69] The Ni−$OPPh_3$ distances in **7** range from 1.9556(14) Å to 1.9700(14) Å, again similar to the lone other complex with this bond type, [(Ph_3PO)$_2$$NiCl_2$], which has two identical Ni−$OPPh_3$ bond distances of 1.966 Å.[74]

In **6** and **7**, the M−$OPPh_3$ bonds are 0.09 Å longer than M−OC_4F_9 bonds at in **6**, and 0.06 Å longer for **7**. This result is in contrast to the PPh_3 complexes, in which the differences in M−P versus M−O range from approximately 0.3−0.5 Å, and shows the significant reduction in steric pressure upon introduction of the $OPPh_3$ ligand.

Complexes **8** and **10** are also pseudo-tetrahedral complexes, with two phosphine groups and one bidentate pin^F ligand, whose ORTEPs are shown in Figures A.2 and A.3, respectively. As in **1** and **3**, M−P bonds are longer than M−O, and **8** and **10** are highly similar to each other, with nearly identical M−O and M−P distances and a comparable O−M−O angle. In **8**, the Co−PPh_3 distances range from 2.3926(5) Å to 2.4256(5) Å, longer compared to the literature average of 2.23(8) Å. The two Co−O_{pinF} distances within **8** are nearly identical, with an average of 1.92(2), and these are also consistent with the literature average of 1.94(6) Å.[75-78] In **10**, the Zn−PPh_3 distances are consistent with the literature average of 2.47(9) Å. As in **8**, the Zn−O_{pinF} distances are nearly identical, and unremarkable compared to a literature average of 1.94(1) Å.[75, 76]

In contrast to all the structures above, **9** is a pseudo-square planar complex with τ_4 value of 0.10, whose ORTEP shown is at the right of Figure 2. Compared to **3** and **7**, there is less steric bulk in the rigid pin^F ligand of **9**, which permits the square planar geometry favorable for a d^8 metal center. The average Ni−O and Ni−P bonds as well as the O−Ni−O angle are similar to those in **8** and **10**. The Ni−PPh_3 distances in **9** are unremarkable from the aforementioned literature standpoint, and average 0.18 Å shorter than those of **3,** attributed to a smaller pin^F ligand cone angle. Compared to the average Ni−O_{pinF} distance in the literature of 1.90(7) Å,[76, 79,

[80] those of **9** are unexceptional. This compound is only the second instance of a heteroleptic Ni-pin^F complex, the first being $[(py)_3Ni(pin^F)]$ (py = pyridine).[79]

Comparing square-planar **9** to previously published square planar complexes *trans*-$[(PPh_3)_2Ni(Ar)_2]$ (Ar = OC_6F_5, or 3,5-$OC_6H_3(CF_3)_2$),[81] the Ni−O bond distances in the OC_6F_5 complex are comparable to those in **9**; however, Ni−P distances in this complex are an average of 0.07 Å longer. There is also a more rigorously square planar center in the OC_6F_5 complex, with angles around Ni nearly 90° and 180°, lacking the geometric constraint that pin^F has in **9.** The $OC_6H_3(CF_3)_2$ complex has more distortion, with distances and angles around Ni more comparable to **9**, which may be attributed to the larger steric bulk of the CF_3 groups on the aryloxides.[81] As expected for complexes with pin^F, the O−M−O angle in **9** is smaller than for OC_4F_9 complexes **1**, **3**, and **6**. This angle is otherwise unremarkable and is in agreement with that of previously published $[M(pin^F)_2]^{2-}$ complexes.[76]

Elongation of the C−C bond in the chelated pin^F backbone is always observed, with typical C−C bond lengths ranging from 1.54(2) Å up to 1.657(3) Å,[76] and is also seen in **8**-**10**, which have an average C−C bond distance of 1.65(2) Å. These data show that this bond length behavior is not exclusive to homoleptic ligand composition of the aforementioned complexes nor a single geometry (tetrahedral or square planar). As previously proposed, this C−C bond elongation may be due to steric repulsion within the CF_3 groups of the pin^F ligand when coordinated to a metal center.[76]

In the solvate **11**, only molecular connectivity was confirmed (Figure A.4), but compositional confirmation was provided by elemental analysis. This structure shows two five coordinate Co^{II} centers bridged by two O atoms from two pin^F ligands. Each Co center is coordinated two THF molecules, both O atoms of one pin^F ligand, as well as an O atom from the second, bridging pin^F ligand. The structure of **12** is proposed to have similar bridging pin^F ligands, with Zn in a pseudo-tetrahedral environment, with composition also confirmed analytically. To our knowledge, **11** and **12** are the first characterized examples of a bridging pin^F ligand.

Electronic structure

Phosphine complexes of the form $[(L)_2M(OR)_2]$, **1**-**3** and **6**-**9**, have an intense UV band at 260 nm, arising from π-donation as alkoxide ligand to metal charge transfer (LMCT). Complex **11** also has a UV band around 260 nm, again from alkoxide LMCT. Solvated **5** was the exception, with weaker UV bands at 231 nm (ε= 232 $M^{-1}cm^{-1}$), and a shoulder at 288 nm (ε= 86 $M^{-1}cm^{-1}$), possessing UV extinction coefficients significantly lower than Fe^{II} complexes **1** (Figure A.5) and **6** (Figure A.6) as well as those of other complexes in this series (Figure A.7). While pseudo-tetrahedral d^6 complexes are expected to have visible transitions, none were observed for Fe^{II} complexes **1**, **5** and **6**, which is unusual.

Co^{II} complexes **2**, **8** and **11** (data shown in Figures A.8 (**2**), A.9 (**8**), and A.10 (**11**)) and Ni^{II} complexes **3**, **7**, and **9** (visible transitions in Figure 3, UV in Figures A.11 (**3**), A.12 (**7**) and A.13 (**9**) all exhibited weak, visible bands indicating *d*−*d* transitions, as expected. For Zn^{II} complexes **4** and **10**, high energy charge-transfer bands were detected and no *d*−*d* bands were observed as expected for a d^{10} complex (Figures A.14 and A.15).

Table 2. Summary of magnetic moment and τ_4 values for complexes **1-11**.

Complex	μ_{eff}	μ_{so}	τ_4
1	4.48(4)	4.90	0.81
2	4.0(1)	3.88	–[b]
3	3.27(8)	2.83	0.83
4	–[a]	0	0.88[35]
5	4.67(7)	4.90	–[b]
6	4.2(1)	4.90	0.79
7	3.07(8)	2.83	0.73
8	4.2(3)	3.88	0.78
9	–[a]	0	0.10
10	–[a]	0	0.83
11	3.07(5)	3.88	–[b]

[a] Diamagnetic.
[b] No structural data.

Solution-state magnetism was evaluated using the Evans method[64, 65] on all complexes except diamagnetic complexes, which are the Zn^{II}-containing **4** and **10**, and square planar Ni^{II}, **9**. These susceptibility values, along with predicted μ_{so} and previously discussed τ_4 values, can be found in Table 2. The ^{1}H-NMR spectra used to determine solution magnetic moments for the paramagnetic compounds can be found in Figures A.16A – A.16H. These μ_{eff} values are unitless, despite being frequently reported in units of Bohr magneton.[82, 83] Fe^{II}-containing **1**, **5** and **6** have μ_{eff} values lower than both the spin-only predicted magnetic moment of 4.90, perhaps due to distortions from purely tetrahedral geometry. Higher values than spin-only ones were observed for the Ni^{II} complexes **3** and **7**, possibly due to weak spin-orbital coupling. The Co^{II} complexes **2** and **8** have μ_{eff} values that are insignificantly higher than the spin-only magnetic moment, with the difference possibly due to experimental error or standard second-order deviations from the spin-only values. The five-coordinate Co^{II} dimer **11** has a μ_{eff} value lower than the predicted μ_{so} value for a high spin d^7 metal center, likely due to antiferromagnetic coupling between the two Co atoms.

Interestingly, when **3** was cooled to −80 °C in THF, the purple solution turned a pale peach color, and the process was reversed by warming back to room temperature. This phenomenon was not observed in related Ni^{II} complexes **7** and **9**. To evaluate this unique behavior of **3**

further, the change in chromophores was probed between −80 °C and room temperature with time-dependent measurements (Figure 4). In THF, there were two visible transitions, at 454 nm and 554 nm, along with a shoulder at 356 nm (black trace). Upon cooling to low temperature over 10 min, the feature at 454 nm grew by 16.9% into a slightly blue-shifted feature at 448 nm with a shoulder at 425 nm. Meanwhile, the feature at 554 nm decayed by 58.1% to 546 nm, again slightly blue-shifted.

This phenomenon was shown to be reversible, as temperature dependent measurements were taken at 20 °C intervals back up to 0 °C, during which time the chromophores reversed to their initial values and peak shape (Figure A.17). Comparing spectra before (solid black trace in Figure 4) and after (dotted trace in Figure 4), the chromophore changes were mostly reversible, though the spectra reveal a slight decay: at 554 nm, there is 81% reversibility while at 454 nm, 94% reversibility (3 nm blue shift to 451 nm after). Notably, related Ni^{II} complexes **7** and **9** did not exhibit this behavior.

In order to further investigate the electronic structure of the low temperature species, Evans method experiments[64, 65] were performed in d_8-THF spiked with hexamethyldisiloxane (HMDSO) at room temperature, −80 and −100 °C. At room temperature, the μ_{eff} is 3.19(4), which was consistent with the aforementioned measurement in CD_3CN (Table 2). At −80 °C, the sample internal HMDSO peak shifted to a more negative value, indicating an even more paramagnetic Ni^{II} center, corresponding with a μ_{eff} value of 4.30(4), assuming there is no compositional change. This shift was even larger at a lower temperature of −100 °C, corresponding with μ_{eff} of 4.59 (one measurement at this temperature) (Figure A.18). These low temperature μ_{eff} values were both slightly higher than is typically observed[84], but still consistent with ~ T_d d^8 Ni^{II}. Notably, the Evans method measurements before and after the experiment were identical (Figure A.19).

Variable-temperature ^{31}P NMR measurements were also performed. Free PPh_3 has a singlet at −5 ppm.[85] At room temperature, the ^{31}P spectrum for **3** revealed a broad feature at −5.55 ppm,

which at −80 °C, shifted to −8.12 ppm and changed to a sharp singlet. At −100 °C, this peak shifted further negative to −8.64 ppm (Figure A.20). These changes indicate a subtle change in phosphorus environment. Since there was only one slightly shifted phosphine peak at low temperature, the PPh_3 groups likely have approximately the same environment, remaining coordinated to the Ni^{II} center.

The combined variable-temperature UV-vis, magnetism, and ^{31}P NMR measurements indicate a change to the environment of the Ni^{II} center. We propose that at low temperature, **3** has a less distorted tetrahedral structure, whereas the room temperature structure moved closer to square planar, as seen in both **9** and the aforementioned previously characterized $[(Ph_3P)_2Ni(OAr)_2]$ complexes (Scheme 3).[81] This equilibrium was limited by the steric bulk of both PPh_3 and OC_4F_9 ligands. As shown in the above experiments, this equilibrium was reversible, with approximate T_d geometry being favored at low temperature, whereas a structure closer to D_{4h} was favored at room temperature. The weak coordination of THF at low temperature is unlikely due to the large steric bulk of the ligands, particularly the fluorinated OC_4F_9 ligands.

Although the electronic spectrum appeared to show a slight decay in **3** before and after cooling (as previously described in Figure 4), the Evans method measurements before and after the experiments were identical (Figure A.19), confirming reversibility. Therefore, this discrepancy between the two electronic spectra was attributed to a slight leak in the septum-sealed cuvette due to the small vacuum created by decreased temperature. Additionally, this equilibrium hypothesis is further supported by ^{31}P NMR, which suggests that both PPh_3 ligands maintain the same coordination regardless of temperature.

Complex reactivity with O_2

There are multiple unknowns in the reactivity that might be observed between O_2 and these new heteroleptic fluorinated alkoxide complexes, including (i) oxidation of PPh_3 or not (ii) binding or

not of any $OPPh_3$ formed, (iii) stoichiometry of any $\{M_xO_y\}$ intermediates and (iv) type of intermolecular substrate oxidation observed.

As seen in our Cu−O_2 work, PPh_3 coordinated to Cu^I was stoichiometrically oxidized upon addition of O_2 and did not associate with the $\{Cu_xO_y\}$ intermediate afterwards. However, this might not be the case for these new studies, as $OPPh_3$ could also coordinate back to Fe after oxidation, or PPh_3 could simply dissociate.

The presence of two PPh_3 ligands in the coordination sphere may allow PPh_3 to be oxidized and dissociate, encouraging facile reduction of O_2 by the low coordination metal centers left behind. In order to assess the ability of PPh_3 to serve as a leaving group in this way several complexes were evaluated for reactivity with O_2. Complexes in this series with Fe, Co and Ni metal centers were screened for their abilities to reduce O_2, to evaluate differences in reactivity influenced by metal center, monodentate versus bidentate ligand coordination, and the presence of reactive PPh_3 versus non-reactive $OPPh_3$ or DME.

A control reaction with Zn complex **4** was first performed by exposing a THF solution of **4** to O_2. After analysis by ^1H NMR, the spectrum was identical to that of the material before O_2 exposure, confirming that neither this complex, nor the PPh_3 ligands, reacted with O_2.

Fe^{II} complex reactivity with O_2

As previously mentioned, when Fe^{II} is exposed to O_2 in non-heme complexes, product oxidation states can be Fe^{III} or Fe^{IV}, and Fe coordination numbers are typically five to six.[3, 4] The typical electronic structure of mononuclear intermediates includes $\{Fe^{III}(\eta^2\text{-}O_2)\}$ peroxo and –superoxo species, as well as Fe^{IV} and Fe^{V}-oxo moieties, whereas that of diiron intermediates are $\{Fe^{III}_2(\mu\text{-}\eta^1\text{:}\eta^1\text{-}O_2)\}$ peroxo, $\{Fe^{II}Fe^{III}(\mu\text{-}\eta^1\text{:}\eta^2\text{-}O_2)\}$ superoxo, and the oxo-containing $\{Fe^{IV}_2((\mu_2\text{-}O)_2\}$, and $\{Fe^{III}Fe^{IV}(\mu_2\text{-}O)_2\}$.[3, 42] The Fe complexes in this series were first evaluated due to the observed air-sensitivity of **1** and **6**. When **1** was exposed to O_2 at −78 °C in THF, yellow-orange species

formed that demonstrated negligible reactivity with H_2Q and PPh_3. Upon warming to room temperature, a clear orange color persisted.

Reactivity of **1** with O_2 was evaluated by UV-vis spectroscopy (Figure 5). Before O_2 addition, **1** had an initial LMCT band at 262 nm. At −80 °C, O_2 was bubbled in for 1 min, and then the solution was monitored spectroscopically every 7 minutes until the spectrum stopped changing. As seen in Figure 5, the LMCT band blue shifted slightly with each measurement, resulting in a broad chromophore at 241 nm. Upon warming the reaction to room temperature, this chromophore persisted, with a 20.3% decay determined by a decrease in absorbance, as shown with the dashed line in Figure 5.

After concentration, the resulting species was a dark orange oil. Stirring this oil in hexanes and triturating resulted in an orange powder. About half of this product dissolved into Et_2O and was layered with hexanes, to afford small orange crystals. The remaining yellow-orange solids were insoluble in the above organic solvents and THF.

Single crystal X-ray diffraction analysis revealed the identity of this Et_2O-soluble product to be $[(F_9C_4O)_2(Ph_3PO)Fe^{III}(\mu_2{-}O)Fe^{III}(OPPh_3)(OC_4F_9)_2]$ (**13**) (Figure 6). Two distorted tetrahedral Fe^{III} centers each bound to two OC_4F_9 groups and one $OPPh_3$ ligand are bridged by O^{2-}. The presence of $OPPh_3$ revealed that at least one PPh_3 ligand from **1** was oxidized by O_2, and this resulting $OPPh_3$ again coordinated to the Fe centers.

Full crystallographic data collection parameters are in Table A.1 and selected distances and angles are in Table 3. The Fe-μ-O distance is 1.7553(7) Å and the Fe atom has a slightly distorted tetrahedral environment, with a τ_4 value of 0.92. The Fe−O−Fe angle is crystallographically constrained to be linear. When looking along the axis of the Fe−O−Fe bond, the ligands around the Fe center are in a staggered conformation, which is expected due to steric bulk.

Table 3. Selected distances (Å) and angles (°) of **13**.

Bond	Distance	Atoms	Angle

Fe−O(1)	1.923(4)	O(1)−Fe−O(2)	103.91(17)
Fe−O(2)	1.866(4)	O(1)−Fe−O(3)	104.38(17)
Fe−O(3)	1.864(4)	O(1)−Fe−O(007)	109.10(12)
Fe−O(007)	1.7553	O(2)−Fe−O(3)	107.5(2)
		O(2)−Fe−O(007)	115.54(16)
		O(3)−Fe−O(007)	115.29(12)
		Fe−O(007)−Fe^{i}	180

Compound **13** has a distinct sharp feature at 261 nm, and two shoulders at 222 nm and 340 nm when evaluated by UV-vis in Et_2O (Figure A.21). The LMCT feature at 261 nm is consistent with those observed in **1**-**11**. The solution state magnetic susceptibility, μ_{eff}, is 2.0(1), significantly lower than the spin-only predicted value for an Fe^{III} high spin tetrahedral complex of 5.92, due to antiferromagnetic coupling through the μ−O moiety. This Fe −(μ−O)−Fe moiety has been widely reported and has been reviewed.[86] Seven other related complexes have a dimer of four- Fe centers bridged by an oxo group. From these complexes, the average distance is 1.78(1) Å, revealing that this distance in **13** is unremarkable. Out of these, only two have a linear Fe−O−Fe central angle. One of these complexes, $\{K(18C6)\}_2[(OAr^F)_3Fe(\mu_2-O)Fe(OAr^F)_3]$, has two Fe^{II} centers which are surrounded by OC_6F_5 ligands. and has two identical Fe−(μ−O) distances of 1.763 Å, comparable to **13**.[87] The other complex, $\{(HNEt_3)_2[Fe(L)(\mu_2-O)Fe(L)]\}$, in which L is the triphenylamine-based 2,2′,2″-nitrilotribenzoic acid, has two Fe^{III} centers each coordinated to three carboxylate groups of a tridentate triphenylamine ligand.[88] Structurally, there are two identical Fe−(μ−O) distances of 1.769 Å, again similar to **13**. Compared to **13**, in which the source of the bridging oxo is O_2, the presence of a bridging oxo unit in both of these complexes is described as a result of the presence of trace H_2O in the reaction.[87, 88] The remaining five complexes have bent Fe−(μ−O)−Fe angles ranging from 133.3° to 177.36°.[89-92]

In the reaction of **1** with O_2, PPh_3 proved to be a successful leaving group, with at least one equivalent oxidized when O_2 is introduced into the reaction solution. Previously, addition of

$OPPh_3$ was found to extend the lifetime of μ-peroxo-$Fe^{III}Fe^{III}$ moiety in multidentate N/O donor species $[(NEt\text{-}hptb)Fe_2(\mu\text{-}1,2\text{-}O_2)(OPPh_3)_2][BF_4]_3$, allowing a crystal structure to be obtained.[93] As in this example, $OPPh_3$ may have also allowed the stabilization of oxidized product **13**. Since $OPPh_3$ was found to coordinate to the Fe center in **13**, further reactivity was explored with complexes with alternative redox inactive L-donor groups, namely, $[(DME)Fe(OC_4F_9)_2]$, **5** and $[(Ph_3PO)_2Fe(OC_4F_9)_2]$, **6**. At −78 °C, when O_2 was introduced directly into solution for 1 min, a pale yellow chromophore was quickly observed, labeled as **5-O_2** and **6-O_2**, respectively. Visible transitions corresponding to strong LMCT bands were nearly identical for both of these solutions 5 min after O_2 introduction, extending to 500 nm, suggesting that these yellow solutions are similar species (Figure A.22). Over 25 min following O_2 introduction, in both cases, this chromophore broadened and red-shifted and then persisted at room temperature. Again, comparing LMCT bands in the visible region, these spectra were nearly identical, absorbing in the range 500- 550 nm (Figure A.23). Additionally, these bands were different than those of **1** with O_2, suggesting that different reactivity occurred in **5** and **6** influenced by lack of ligand oxidation ($OPPh_3$ or DME), or that different ligand sets may alter the Fe energy levels. Attempts to identify the final oxidized products of **5** and **6** analogous to **13** were unsuccessful, but the yellow color suggests oxidation to Fe^{III} occurred. Comparing the LMCT bands that extend into the visible region with those of **1** after exposure to O_2 at room temperature, **5** and **6** were less broad, but all three extend to around 600 nm (Figure A.24). This suggests that the final oxidized products may be similar in all cases.

Since a potentially reactive intermediate was observed for reaction of both **5** and **6** with O_2, substrate oxidation reactivity was explored (Table 4). Possible oxidase reactivity was investigated using hydroquinone (H_2Q), previously used in oxidase reactions with $\{Cu_3O_2\}^{3-}$ species.[22, 23] When 10 eq of H_2Q were added to yellow intermediate **5-O_2** at –78 °C, a dark solution was observed, which when warmed to room temperature was a clear solution with

black precipitate. After quenching with HCl and extracting into Et_2O, ^1H NMR studies revealed stoichiometric oxidation of H_2Q, with an average TON of 1.0(1) (per Fe). Similar observations were made for H_2Q oxidation by **6-O₂**, with an average TON of 1.2(1), as summarized in Table A.3. Additionally, a control reaction was run with **13** in order to evaluate possible H_2Q oxidation by Fe(III). This reaction was run by first oxygenating **1** to make **13**, and the control proceeded with crude material for the substrate analysis. No BQ was detected, confirming that this solution did not perform oxidase catalysis; however, the recovered yield of H_2Q was lower than expected (45%), suggesting that some additional unknown reactivity may have occurred.

Thioanisole (PhSMe) was used to probe oxygen atom transfer (OAT) capabilities.[4, 94-97] When 5 eq of PhSMe were added to **5-O₂** at –78 °C, the solution remained a pale yellow over 30 min. Upon warming the reaction flask to room temperature, the solution appeared the same by eye as spectroscopic samples yellow-orange. After quenching with HCl and removing THF, the organic materials were extracted into CH_2Cl_2. ^1H NMR studies revealed that there was sub-stoichiometric conversion of PhSMe to methyl phenyl sulfoxide at 7.0%, with 22.4% PhSMe recovered. Low PhSMe recovery was attributed to PhSMe lost during concentration steps in work-up. Studies of **6-O₂** led to very similar observations, and when evaluated by ^1H NMR, demonstrated 19.3% sub-stoichiometric conversion to the sulfoxide, with 43.6% of PhSMe recovered.

Table 4. Summary of substrate oxidation reactions in THF at −78° C with 5 mM Fe^{II}, with $Fe(OTf)_2$ and **13** included as control reactions.

Fe^{II} Source	Substrate	Fe^{II} (equiv)	Initial substrate (equiv)	Recovered substrate (equiv)	Oxidized product (equiv)	TON (per 1Fe)
5	H_2Q	1.0	10.0	5.0	1.0	1.0
6	H_2Q	1.0	10.0	4.2	1.2	1.2
Fe(OTf)₂	H_2Q	1.0	10.1	6.1	0.1	0.1
13	H_2Q	1.0	10.2	4.7	0	0
5	PhSMe	1.0	5.0	1.1	0.1	0.1
6	PhSMe	1.0	5.0	2.2	0.2	0.2

Both **5-O_2** and **6-O_2** were unreactive with 9-fluorenol, a possible hydrogen atom transfer (HAT) source. Possible aromatic C-H hydroxylation or C−C coupling were evaluated by introduction of sodium 2,4-di-tert-butylphenolate, NaDBP, to **6-O_2**, followed by warming to room temperature, quenching with HCl, removing THF, and extraction of product into CH_2Cl_2, the product was evaluated by ^{1}H NMR. However, the resulting spectrum showed no clear evidence for either oxidation.

The low yields in intermolecular oxidation reactivity and short lifetimes suggest that both **5-O_2** and **6-O_2** are {Fe_nO_x} reactive species, but react preferentially with solvent under these conditions. To identify reactive species **5-O_2** and **6-O_2**, reaction conditions must be optimized. Fe^{II} precursor complexes **1**, **5**, and **6** are neutral species, not stabilized by cation···F/O interactions. Our work investigating Cu^{I} alkoxide complexes has shown that the availability of these interactions influences the ability of Cu^{I} to reduce O_2, and so this concept could be extended to this series.[21] Previous {Fe_xO_y} investigations showed that these intermediates have coordination numbers of five and six[3, 4], so these {$M(OR^F)_2$} complexes could be too under-coordinated to stabilize such an intermediate. Further investigation could include different solvents, lower temperatures, and change in phosphine stoichiometry and identity. Incorporation of a cation could also be considered, either through complex redesign or addition of a salt with a non-coordinating anion.

Co^{II}- and Ni^{II} complex reactivity with O_2

O_2 reactivity with Fe complexes **1**, **5**, and **6** revealed the success in using an L-donor ligand as a protecting group, stabilizing the low-coordinate {$M(OR)_2$} fragments under inert conditions. As a result, Co^{II} and Ni^{II} complexes of this series were also investigated for O_2 reactivity.

Co^{II} complex **2** showed no reactivity with O_2 at –78 °C or room temperature, unsurprising for a Co^{II} complex with O-donors. Since **2** did not exhibit O_2 reactivity, reduction to Co^{I} was attempted by combining **2** with cobaltocene ([Cp_2Co]) in THF, which led to a dark green solution. Recrystallization afforded green crystals suitable for X-ray analysis, but were found to be

$[Cp_2Co][Co(OC_4F_9)_3(THF)]$,[98] which have been deposited to the CSD. This product revealed that a reduced Co^{I} complex was unstable in this ligand environment and maybe have rearranged upon electron loss, losing PPh_3 in the process. This complex is the $[Cp_2Co]^+$ version of the previously published $\{K(18C6)\}[Co(OC_4F_9)_3(THF)]\}$.[62]

To evaluate the effect of ligand on O_2 addition, Co-containing **8** was evaluated in CH_2Cl_2, as exposure of **8** to THF results in rearrangement into **11**. Unlike **2**, **8** turned a pale blue, indicating that less steric bulk may allow reduction of O_2, likely by oxidation of PPh_3. Investigation by UV-vis spectroscopy revealed that upon exposure to O_2 at –80 °C, the initial chromophores at 585 nm and 638 nm remained the same, with the feature at 585 nm slightly decreasing in intensity while that at 638 nm slightly increases (Figure ~~A.24~~A.25). Upon warming the solution to room temperature, a significant drop in relative absorbance (~0.8) was observed, with a new feature at observed at 611 nm and shoulders at 540 and 660 nm. No oxidized species were able to be identified.

In inorganic complexes, Ni^{II} is known to be largely air-stable, and reduction of O_2 alone to reach Ni^{III} is unusual.[56, 99, 100] This oxidation becomes more favorable when Ni^{II} has electron-rich ligands, which are able to lower the redox potential.[60] Surprisingly, when Ni^{II}-containing **3** was exposed to O_2 in THF at room temperature, the color slowly changed to pale green over 10-15 minutes. UV-vis studies revealed the disappearance of chromophores for **3** and the growth of a distinct feature at 452 nm and a broad feature at 700 nm (Figure ~~A.25~~A.26). After concentration and trituration, a green and white powder remained. The white powder was extracted into Et_2O, and then evaluated by ^1H NMR. The powder was shown to consist of PPh_3 recovered at 57.8%, as well as $OPPh_3$, recovered at 15.4%. The green material was unable to be identified, and likely contained the remaining PPh_3 and/or $OPPh_3$. There was no evidence as to whether or not Ni^{II} was also oxidized. Oxidation of Ni^{II} by O_2 is unusual, as discussed above, and would have to be investigated further to confirm.

When **3** was cooled to −80 °C, the solution turned from purple to peach-pink, as previously discussed, and when O_2 was introduced, the solution turned yellow, characterized by broad visible chromophores at 451 and 544 nm (Figure ~~A.26~~A.27). After warming to room temperature, the yellow color persisted, distinct from the oxidized product of exposure of **3** to O_2 at room temperature. The concentrated species was oily and was unable to be crystallized or identified. UV-vis spectroscopy studies were performed to evaluate reactivity of **3** with O_2 under both room temperature and low temperature conditions, confirming spectroscopic differences (Figures ~~A.25~~A.26 and ~~A.26~~A.27). There are two possibilities: (1) differences in symmetry of **3** effects different products upon O_2 reduction; or (2) like **3**, the products of the oxidation reaction could have chromophores sensitive to symmetry changes.

The Ni-pin^F-containing **9** also turned pale green when exposed to O_2, suggesting that a similar reaction happens to that of **3**, possibly due to similar $Ni^{III/II}$ redox potentials in both **3** and **9**. The formation of a pale green oxidized product upon addition of O_2 in both **3** and **9** also suggests that fluorinated ligand cone angle does not affect product formation in the Ni^{II} case, as opposed to the Co^{II} complexes.

Overall, the O_2 reactivity of nearly all complexes in this series reveals that PPh_3 can effectively fill the coordination sphere of fluorinated alkoxide complexes in an inert environment. Upon addition of O_2, these ligands either leave or are oxidized and dissociate, resulting in lower coordination numbers at the metal center that may promote reduction of O_2. Substituting PPh_3 on Fe^{II} with non-reactive DME (**5**) or $OPPh_3$ (**6**) resulted in observation of a distinct possible reactive species immediately upon O_2 addition that was unable to be stabilized. It must be considered that this could also simply be the oxidation of Fe^{II} to Fe^{III} and not an intermediate. While O_2 reactivity is also observed in Co^{II}-containing **8** and Ni^{II}-containing**3** and **9**, it is unknown whether solely PPh_3 is oxidized and the 3*d* center rearranges, or if the 3*d* center also reduced O_2.

Further work to characterize reactive species must be performed, through either addition of a cation source to add potentially stabilizing cation···F/O interactions, or through complex redesign, through the incorporation of a cation and/or having only one phosphine group, as described above.

Conclusions

In order to assess the efficacy of phosphine as a protecting group for low coordinate fluorinated {$M(OR)_2$} fragments, in oxidation reactions with O_2, a series of heteroleptic [$L_2M(OR)_2$] complexes with 3*d* metal centers was synthesized. The synthesis of these complexes was straightforward, resulting in complexes with largely unexceptional geometries and electronic structures. The Ni^{II} complex [$(Ph_3P)_2Ni(OC_4F_9)_2$], **3**, had unique electronic structure behavior, with quasi D_{4h} structure at room temperature, and quasi T_d structure at low temperature. The related complex [$(Ph_3P)_2Ni(pin^F)$], **9**, had a more square planar geometry, due to less steric hindrance of the pin^F ligand compared to that of the OC_4F_9 ligand. This series of complexes was then evaluated for reactivity with O_2. Oxidized product **13**, $[(F_9C_4O)_2(Ph_3PO)Fe(\mu_2{-}O)Fe(OPPh_3)(OC_4F_9)_2]$, was identified from oxidation of $[(Ph_3P)_2Fe(OC_4F_9)_2]$. When related Fe^{II} complexes **5** and **6** were evaluated, short-lived pale yellow intermediates were identified which were able to perform stoichiometric oxidase conversion of hydroquinone to benzoquinone, and sub-stoichiometric OAT in the oxidation of thioanisole to methyl phenyl sulfoxide. When the Co^{II} complexes were evaluated, the $[(Ph_3P)_2Co(OC_4F_9)_2]$ complex, **2**, did not react, whereas the $[(Ph_3P)_2Co(pin^F)]$ complex, **8**, changed color. This difference in reactivity could be due to the pin^F ligand affecting sterics and/or redox activity of the Co^{II} center, which will be explored in the future. Interestingly, both Ni^{II} complexes **3** and **9** have similar reactivity with O_2 despite having different geometries. This suggests that either redox behavior of Ni^{II} is the same in both complexes, or that differences in cone angle between OC_4F_9 and pin^F do not affect O_2 reactivity. Future work will include further

exploration of differences in Co^{II} reactivity with O_2, as well as efforts to stabilize $\{M_xO_y\}$ intermediates that can perform substrate intermolecular oxidation.

Acknowledgements

We gratefully acknowledge the financial support of the NSF (CHE 01800313 to LHD, CHE 0619339 to BU for NMR spectrometer) and BU (Mason Memorial Fund for VLH) for financial support. We thank Jessica K. Elinburg for synthetic assistance involving Ni complexes.

Appendix A: Supplementary Data

CCDC 1980240-1980247 depositions contain the supplementary crystallographic data for **1**, **3**, **6**-**10** and **13**. This data can be obtained free of charge at http://www.ccdc.cam.ac.uk/conts/retrieving.html, or from the Cambridge Crystallographic Data Centre, 12 Union Road, Cambridge CB2 1EZ, UK; fax: (+44) 1223-336-033; or e-mail: deposit@ccdc.cam.ac.uk. The supplementary information also contains additional ORTEP diagrams, structural information, and electronic structure data.

References

1. A. Decker and E. I. Solomon, *Curr. Opin. Chem. Biol.*, 2005, **9**, 152-163.
2. T. L. Poulos, *Chem. Rev.*, 2014, **114**, 3919-3962.
3. A. J. Jasniewski and L. Que, *Chem. Rev.*, 2018, **118**, 2554-2592.
4. M. Costas, M. P. Mehn, M. P. Jensen and L. Que, *Chem. Rev.*, 2004, **104**, 939-986.
5. M. M. Abu-Omar, A. Loaiza and N. Hontzeas, *Chem. Rev.*, 2005, **105**, 2227-2252.
6. E. G. Kovaleva and J. D. Lipscomb, *Nature Chemical Biology*, 2008, **4**, 186-193.
7. R. L. Peterson, S. Kim and K. D. Karlin, in *Comprehensive Inorganic Chemistry II (Second Edition)*, ed. K. Poeppelmeier, Elsevier, Amsterdam, 2013, DOI: https://doi.org/10.1016/B978-0-08-097774-4.00309-0, pp. 149-177.
8. S. M. Adam, G. B. Wijeratne, P. J. Rogler, D. E. Diaz, D. A. Quist, J. J. Liu and K. D. Karlin, *Chem. Rev.*, 2018, **118**, 10840-11022.
9. C. E. Elwell, N. L. Gagnon, B. D. Neisen, D. Dhar, A. D. Spaeth, G. M. Yee and W. B. Tolman, *Chem. Rev.*, 2017, **117**, 2059-2107.
10. L. M. Mirica, X. Ottenwaelder and T. D. P. Stack, *Chem. Rev.*, 2004, **104**, 1013-1045.
11. E. A. Lewis and W. B. Tolman, *Chem. Rev.*, 2004, **104**, 1047-1076.
12. G. I. Pannov, V. I. Sobolev and A. S. Kharitonov, *J. Mol. Catal.*, 1990, **61**, 85-97.
13. M. H. Groothaert, P. J. Smeets, B. F. Sels, P. A. Jacobs and R. A. Schoonheydt, *J. Am. Chem. Soc.*, 2005, **127**, 1394-1395.
14. B. E. R. Snyder, M. L. Bols, R. A. Schoonheydt, B. F. Sels and E. I. Solomon, *Chem. Rev.*, 2018, **118**, 2718-2768.
15. B. E. R. Snyder, P. Vanelderen, M. L. Bols, S. D. Hallaert, L. H. Böttger, L. Ungur, K. Pierloot, R. A. Schoonheydt, B. F. Sels and E. I. Solomon, *Nature*, 2016, **536**, 317-321.
16. A. J. Knorpp, M. A. Newton, S. C. M. Mizuno, J. Zhu, H. Mebrate, A. B. Pinar and J. A. van Bokhoven, *Chem. Commun.*, 2019, **55**, 11794-11797.
17. M. Ravi, V. L. Sushkevich, A. J. Knorpp, M. A. Newton, D. Palagin, A. B. Pinar, M. Ranocchiari and J. A. van Bokhoven, *Nat. Catal.*, 2019, **2**, 485-494.
18. K. T. Dinh, M. M. Sullivan, K. Narsimhan, P. Serna, R. J. Meyer, M. Dincă and Y. Román-Leshkov, *J. Am. Chem. Soc.*, 2019, **141**, 11641-11650.
19. P. J. Smeets, J. S. Woertink, B. F. Sels, E. I. Solomon and R. A. Schoonheydt, *Inorg. Chem.*, 2010, **49**, 3573-3583.
20. S. E. N. Brazeau and L. H. Doerrer, *Dalton Trans.*, 2019, **48**, 4759-4768.
21. J. S. Lum, L. Tahsini, J. A. Golen, C. Moore, A. L. Rheingold and L. H. Doerrer, *Chem. Eur. J.*, 2013, **19**, 6374-6384.
22. S. F. Hannigan, A. I. Arnoff, S. E. Neville, J. S. Lum, J. A. Golen, A. L. Rheingold, N. Orth, I. Ivanović-Burmazović, P. Liebhäuser, T. Rösener, J. Stanek, A. Hoffmann, S. Herres-Pawlis and L. H. Doerrer, *Chem. Eur. J.*, 2017, **23**, 8212-8224.
23. S. E. N. Brazeau, E. E. Norwine, S. F. Hannigan, N. Orth, I. Ivanović-Burmazović, D. Rukser, F. Biebl, B. Grimm-Lebsanft, G. Praedel, M. Teubner, M. Rübhausen, P. Liebhäuser, T. Rösener, J. Stanek, A. Hoffmann, S. Herres-Pawlis and L. H. Doerrer, *Dalton Trans.*, 2019, **48**, 6899-6909.
24. G. L. Miessler, P. J. Fischer and D. A. Tarr, *Inorganic Chemistry, International Edition*, Pearson Education, Inc., 5th edn., 2014.
25. C. C. C. Johansson Seechurn, M. O. Kitching, T. J. Colacot and V. Snieckus, *Angew. Chem. Int. Ed.*, 2012, **51**, 5062-5085.
26. K. Osakada, T. Takizawa, M. Tanaka and T. Yamamoto, *J. Organomet. Chem.*, 1994, **473**, 359-369.

27. T. H. Lemmen, G. V. Goeden, J. C. Huffman, R. L. Geerts and K. G. Caulton, *Inorg. Chem.*, 1990, **29**, 3680-3685.
28. S. Durini, G. A. Ardizzoia, G. Colombo, B. Therrien and S. Brenna, *Polyhedron*, 2018, **139**, 189-195.
29. D. A. Knight and S. W. Keller, *J. Chem. Crystallogr.*, 2006, **36**, 531-542.
30. Z.-F. Chen, B.-Q. Li, Y.-R. Xie, R.-G. Xiong, X.-Z. You and X.-L. Feng, *Inorg. Chem. Commun.*, 2001, **4**, 346-349.
31. R. D. Hart, P. C. Healy, G. A. Hope, D. W. Turner and A. H. White, *J. Chem. Soc., Dalton Trans.*, 1994, DOI: 10.1039/DT9940000773, 773-779.
32. M. Dunaj-Jurco, M. Koman, D. Valigura and G. Ondrejovic, *Acta Crystallogr. Sect. C: Cryst. Struct. Commun.*, 1995, **51**, 1082-1084.
33. P. E. Chen, J. McNeely, J. S. Lum, E. J. Gardner, V. Phillips, J. A. Golen, A. L. Rheingold and L. H. Doerrer, *Polyhedron*, 2016, **116**, 204-215.
34. P. Tasker, A. Parkin, D. Coventry, S. Parsons and D. Messenger, *CCDC 276830: CSD Communication*, 2005.
35. T. O. Petersen and I. Krossing, *CCDC 1418294: CSD Communication*, 2015.
36. T. O. Petersen and I. Krossing, *CCDC 1418214: CSD Communication*, 2015.
37. T. O. Petersen and I. Krossing, *CCDC 1418222: CSD Communication*, 2015.
38. W. Nam, Y.-M. Lee and S. Fukuzumi, *Acc. Chem. Res.*, 2014, **47**, 1146-1154.
39. C. Krebs, D. Galonić Fujimori, C. T. Walsh and J. M. Bollinger, *Acc. Chem. Res.*, 2007, **40**, 484-492.
40. J. Hohenberger, K. Ray and K. Meyer, *Nat. Comm.*, 2012, **3**, 720.
41. G. E. Cutsail, E. J. Blaesi, C. J. Pollock, J. M. Bollinger, C. Krebs and S. DeBeer, *J. Inorg. Biochem.*, 2020, **203**, 110877.
42. W. Nam, *Acc. Chem. Res.*, 2015, **48**, 2415-2423.
43. A. T. Fiedler and A. A. Fischer, *J. Biol. Inorg. Chem.*, 2017, **22**, 407-424.
44. A. J. Fielding, J. D. Lipscomb and L. Que, *J. Biol. Inorg. Chem.*, 2014, **19**, 491-504.
45. E. C. Niederhoffer, J. H. Timmons and A. E. Martell, *Chem. Rev.*, 1984, **84**, 137-203.
46. R. D. Jones, D. A. Summerville and F. Basolo, *Chem. Rev.*, 1979, **79**, 139-179.
47. D. H. Busch and N. W. Alcock, *Chem. Rev.*, 1994, **94**, 585-623.
48. S. Hikichi, M. Akita and Y. Moro-oka, *Coord. Chem. Rev.*, 2000, **198**, 61-87.
49. X. Hu, I. Castro-Rodriguez and K. Meyer, *J. Am. Chem. Soc.*, 2004, **126**, 13464-13473.
50. O. M. Reinaud, G. P. A. Yap, A. L. Rheingold and K. H. Theopold, *Angew. Chem. Int. Ed.*, 1995, **34**, 2051-2052.
51. J. W. Egan, B. S. Haggerty, A. L. Rheingold, S. C. Sendlinger and K. H. Theopold, *J. Am. Chem. Soc.*, 1990, **112**, 2445-2446.
52. J. L. Boer, S. B. Mulrooney and R. P. Hausinger, *Arch. Biochem. Biophys.*, 2014, **544**, 142-152.
53. S. W. Ragsdale, *J. Biol. Chem.*, 2009, **284**, 18571-18575.
54. P. J. Chirik and K. Wieghardt, *Science*, 2010, **327**, 794-795.
55. J.-L. Pierre, *Chem. Soc. Rev.*, 2000, **29**, 251-257.
56. J. Rajpurohit, P. Shukla, P. Kumar, C. Das, S. Vaidya, M. Sundararajan, M. Shanmugam and M. Shanmugam, *Inorg. Chem.*, 2019, **58**, 6257-6267.
57. J. Cho, R. Sarangi, J. Annaraj, S. Y. Kim, M. Kubo, T. Ogura, E. I. Solomon and W. Nam, *Nat. Chem.*, 2009, **1**, 568-572.
58. S. Yao and M. Driess, *Acc. Chem. Res.*, 2012, **45**, 276-287.
59. J. Cho, H. Y. Kang, L. V. Liu, R. Sarangi, E. I. Solomon and W. Nam, *Chem. Sci.*, 2013, **4**, 1502-1508.
60. M. T. Kieber-Emmons and C. G. Riordan, *Acc. Chem. Res.*, 2007, **40**, 618-625.
61. A. Grass, D. Wannipurage, R. L. Lord and S. Groysman, *Coord. Chem. Rev.*, 2019, **400**, 213044.

62. S. A. Cantalupo, J. S. Lum, M. C. Buzzeo, C. Moore, A. G. Di Pasquale, A. L. Rheingold and L. H. Doerrer, *Dalton Trans.*, 2010, **39**, 374-383.
63. R. A. Heintz, J. A. Smith, P. S. Szalay, A. Weisgerber and K. R. Dunbar, in *Inorg. Synth.*, ed. D. Coucouvanis, 2002, DOI: 10.1002/0471224502.ch2, pp. 75-121.
64. S. K. Sur, *J. Magn. Reson.*, 1989, **82**, 169-173.
65. D. F. Evans, *J. Chem. Soc.*, 1959, 2003-2005.
66. O. V. Dolomanov, L. J. Bourhis, R. J. Gildea, J. A. K. Howard and H. Puschmann, *J. Appl. Crystallogr.*, 2009, **42**, 339- 341.
67. C. J. Willis, *Coord. Chem. Rev.*, 1988, **88**, 133-202.
68. D. C. Bradley, R. C. Mehrotra, I. P. Rothwell and A. Singh, *Alkoxo and Aryloxo Derivatives of Metals*, Academic Press, San Diego, California, USA, 2001.
69. B. N. Zheng, M. O. Miranda, A. G. Di Pasquale, J. A. Golen, A. L. Rheingold and L. H. Doerrer, *Inorg. Chem.*, 2009, **48**, 4274-4276.
70. Z. Ding, S. Bhattacharya, J. K. McCusker, P. M. Hagen, D. N. Hendrickson and C. G. Pierpont, *Inorg. Chem.*, 1992, **31**, 870-877.
71. I. Ondrejkovicova, M. Melnik, K. Smolander and M. Ahlgren, *Acta Chem. Scand.*, 1995, 475.
72. Z. Olejnik, T. Lis and I. Ondrejkovicova, *Acta Crystallogr. Sect. C: Cryst. Struct. Commun.*, 1995, **51**, 2246- 2249.
73. E. Durcanska, T. Glowiak, E. Gyepes, I. Ondrejkovicova and G. Ondrejovic, *Acta Fac. Rer. Nat. U. Com. Chim.*, 1991, **39**, 3.
74. R. Moreno-Fuquen, O. Cifuentes, J. V. Naranjo, L. M. Serratto and A. R. Kennedy, *Acta Crystallogr. Sect. Sect. E: Struct. Rep. Online*, 2004, **60**, 1861-1862.
75. S. A. Cantalupo, S. R. Fiedler, M. P. Shores, A. L. Rheingold and L. H. Doerrer, *Angew. Chem. Int. Ed.*, 2012, **51**, 1000-1005.
76. L. Tahsini, S. E. Specht, J. S. Lum, J. J. M. Nelson, A. F. Long, J. A. Golen, A. L. Rheingold and L. H. Doerrer, *Inorg. Chem.*, 2013, **52**, 14050-14063.
77. X. Wurzenberger, C. Neumann and P. Klüfers, *Angew. Chem. Int. Ed.*, 2013, **52**, 5159-5161.
78. J. L. Steele, L. Tahsini, C. Sun, J. K. Elinburg, C. M. Kotyk, J. McNeely, S. A. Stoian, A. Dragulescu-Andrasi, A. Ozarowski, M. Ozerov, J. Krzystek, J. Telser, J. W. Bacon, J. A. Golen, A. L. Rheingold and L. H. Doerrer, *Chem. Commun.*, 2018, **54**, 12045-12048.
79. S. E. Specht, L. H. Doerrer, A. J. Schnepp and A. L. Rheingold, *CCDC 1011902: CSD Communication*, 2014.
80. D. M. Barnhart and E. C. Lingafelter, *Cryst. Struc. Commun.*, 1982, **11**, 733.
81. M. Kim, L. N. Zakharov, A. L. Rheingold and L. H. Doerrer, *Polyhedron*, 2005, **24**, 1803-1812.
82. J. I. Hoppe, *J. Chem. Educ.*, 1972, **49**, 505.
83. S. Kettle, in *Physical Inorganic Chemistry*, Springer, 1996, pp. 185- 210.
84. F. A. Cotton and G. Wilkinson, *Advanced Inorganic Chemistry* Wiley, New York, 4th edn., 1980.
85. J. Schraml, M. Čapka and V. Blechta, *Magn. Reson. Chem.*, 1992, **30**, 544-547.
86. D. M. Kurtz, *Chem. Rev.*, 1990, **90**, 585-606.
87. S. A. Cantalupo, H. E. Ferreira, E. Bataineh, A. J. King, M. V. Petersen, T. Wojtasiewicz, A. G. DiPasquale, A. L. Rheingold and L. H. Doerrer, *Inorg. Chem.*, 2011, **50**, 6584-6596.
88. S. Wörl, D. Hellwinkel, H. Pritzkow, M. Hofmann and R. Krämer, *Dalton Trans.*, 2004, 2750-2757.
89. F. Liu, K. D. John, B. L. Scott, R. T. Baker, K. C. Ott and W. Tumas, *Angew. Chem. Int. Ed.*, 2000, **39**, 3127-3130.
90. J. A. Bellow, M. Yousif, D. Fang, E. G. Kratz, G. A. Cisneros and S. Groysman, *Inorg. Chem.*, 2015, **54**, 5624-5633.
91. A. Arbaoui, C. Redshaw, M. R. J. Elsegood, V. E. Wright, A. Yoshizawa and T. Yamato, *Chem. Asian J.*, 2010, **5**, 621-633.

92. U. Preiss, W. Beichel, G. Steinfeld, G. S. Quinones and I. Krossing, *CCDC 1015614: CSD Communication*, 2014.
93. Y. Dong, S. Yan, V. G. Young Jr. and L. Que Jr., *Angew. Chem. Int. Ed.*, 1996, **35**, 618-620.
94. J. S. Pap, M. A. Cranswick, É. Balogh-Hergovich, G. Baráth, M. Giorgi, G. T. Rohde, J. Kaizer, G. Speier and L. Que Jr., *Eur. J. Inorg. Chem.*, 2013, **2013**, 3858-3866.
95. M. H. Lim, J.-U. Rohde, A. Stubna, M. R. Bukowski, M. Costas, R. Y. N. Ho, E. Münck, W. Nam and L. Que, *Proc. Natl. Acad. Sci. USA*, 2003, **100**, 3665-3670.
96. C. Duboc-Toia, S. Ménage, R. Y. N. Ho, L. Que, C. Lambeaux and M. Fontecave, *Inorg. Chem.*, 1999, **38**, 1261-1268.
97. H. Srour, P. Le Maux, S. Chevance and G. Simonneaux, *Coord. Chem. Rev.*, 2013, **257**, 3030-3050.
98. A. L. Rheingold, *CCDC 1864400: CSD Communication*, 2018.
99. E. Kimura, A. Sakonaka, R. Machida and M. Kodama, *J. Am. Chem. Soc.*, 1982, **104**, 4255-4257.
100. W. Bal, M. I. Djuran, D. W. Margerum, E. T. Gray, M. A. Mazid, R. T. Tom, E. Nieboer and P. J. Sadler, *J. Chem. Soc., Chem. Commun.*, 1994, 1889-1890.

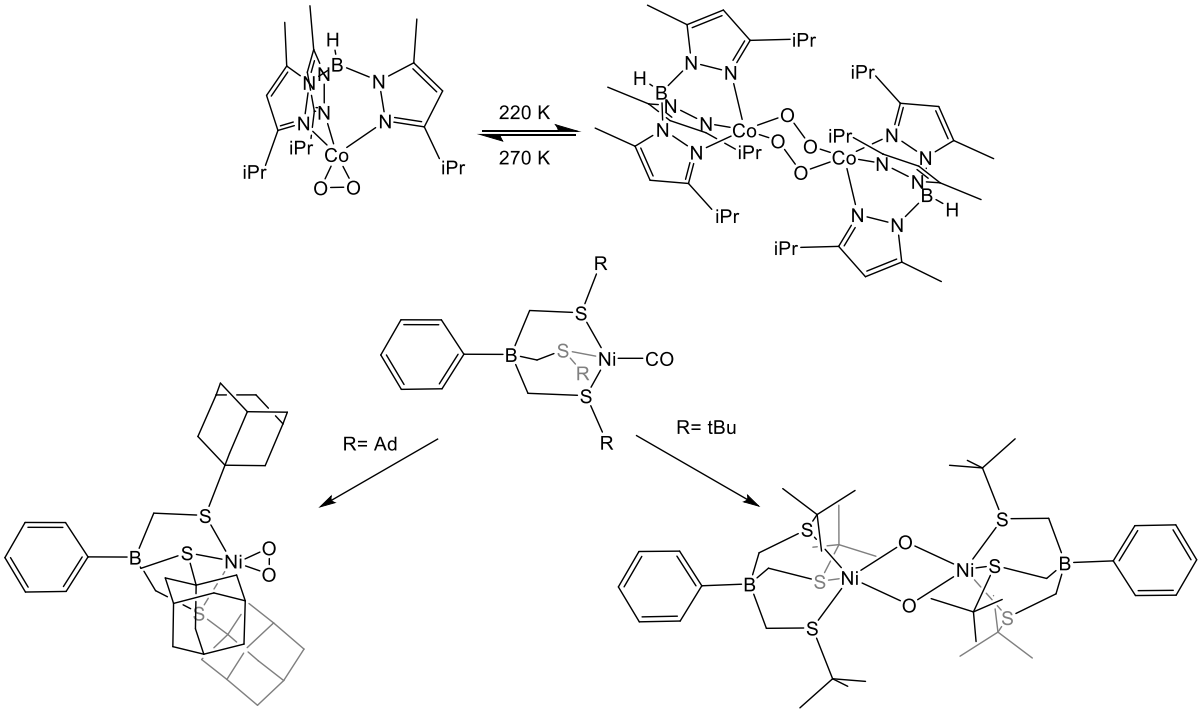

Scheme 1. Examples of $\{Co_xO_y\}$ (top) and $\{Ni_xO_y\}$ (bottom) cores formed upon exposure of reduced *3d* center to O_2.

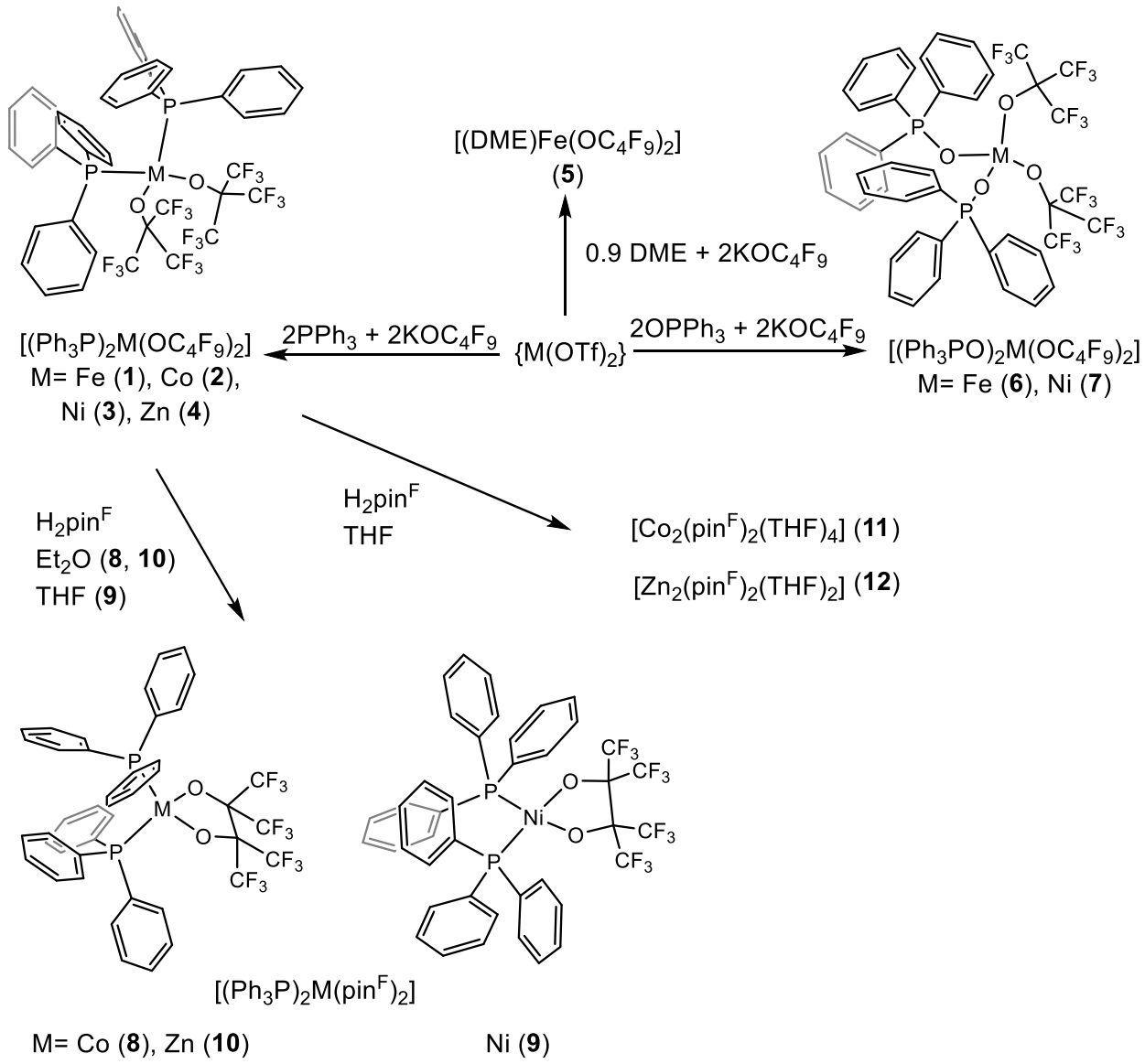

Scheme 2. Syntheses of divalent 3*d* mixed phosphine alkoxide complexes.

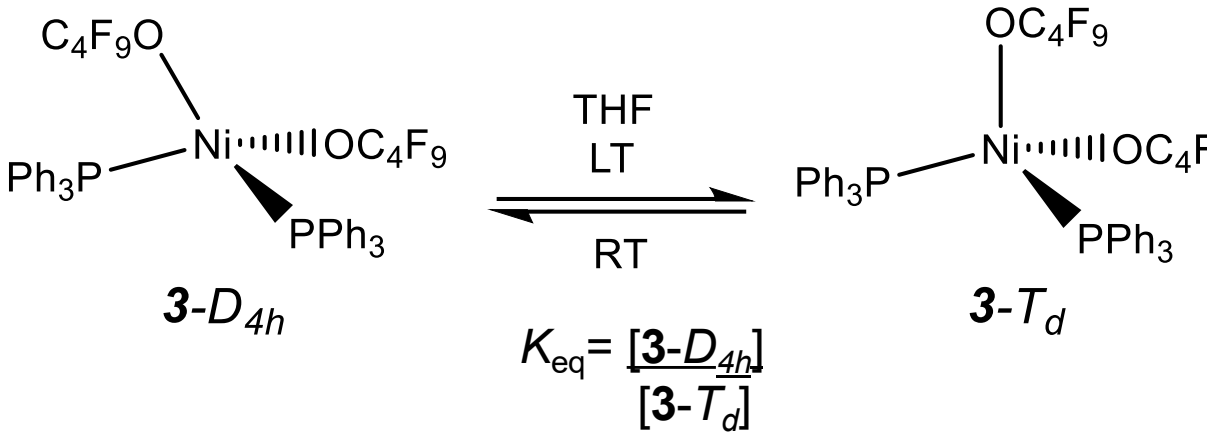

Scheme 3. When **3** is cooled in THF, propose that equilibrium is shifted from ~D_{4h} to ~T_d, which is reversible with temperature.

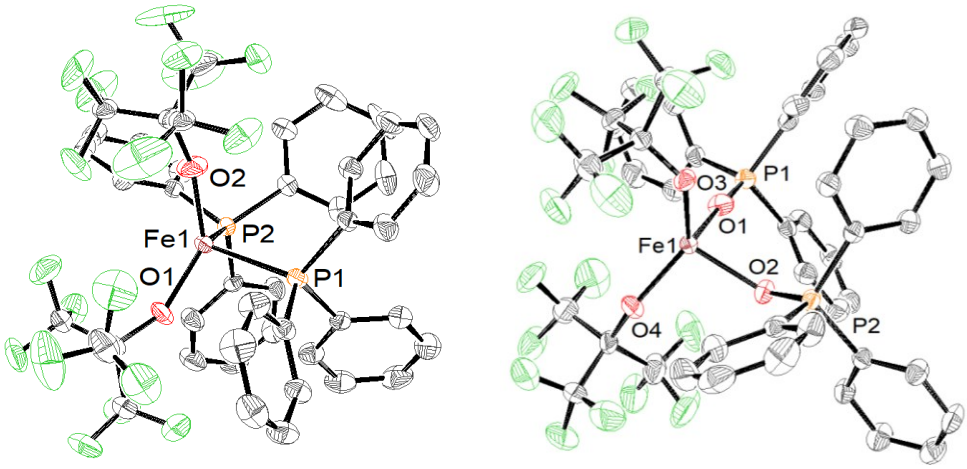

Figure 1. ORTEP diagram of Fe complexes **1** (left) and **6** (right). Fluorine and hydrogen atoms omitted for clarity. Ellipsoids are shown at the 50% probability level.

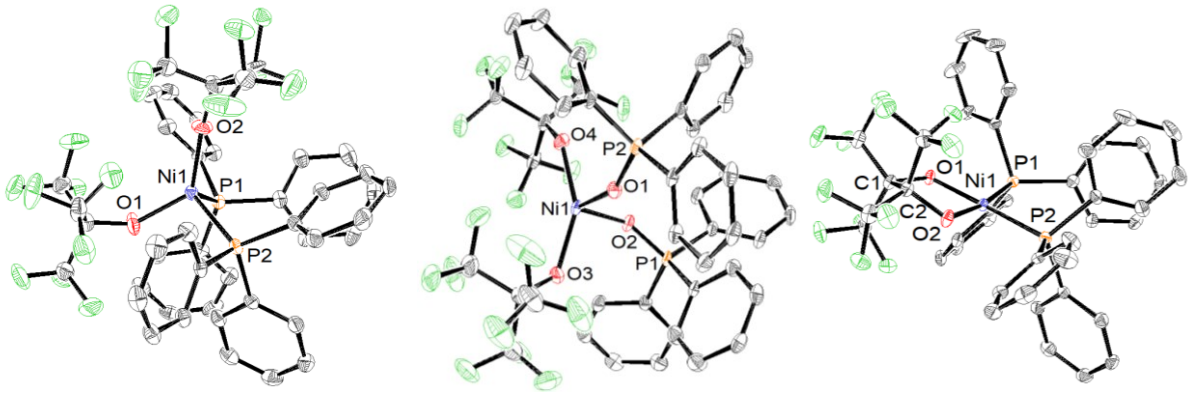

Figure 2. ORTEP diagram of Ni complexes **3** (left), **7** (center) and **9** (right). Some carbon and fluorine atoms were omitted for clarity. Hydrogen atoms were omitted for clarity in all three complexes. Ellipsoids are shown at the 50% probability level.

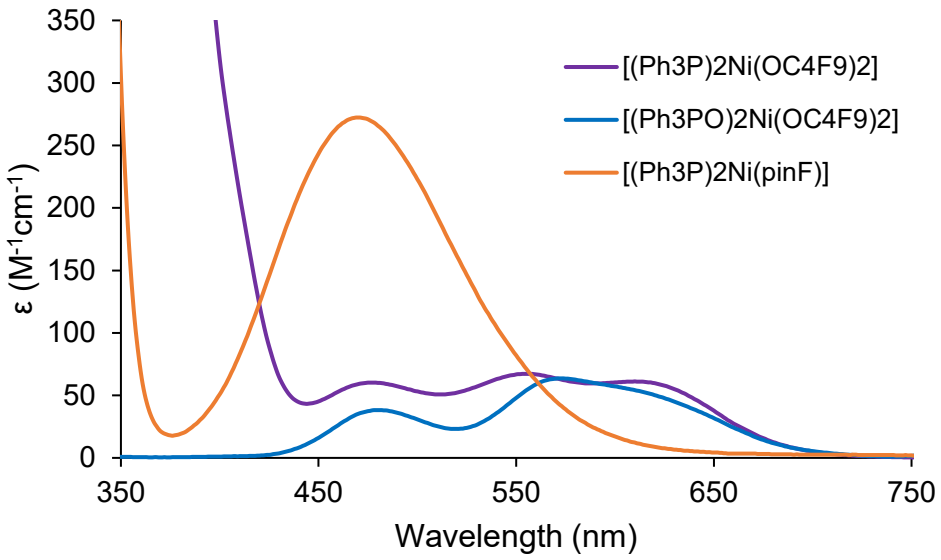

Figure 3. Comparison of *d*−*d* bands for $[(Ph_3P)_2Ni(OC_4F_9)_2]$, (**3**), $[(Ph_3PO)_2Ni(OC_4F_9)_2]$ (**7**), and $[(Ph_3P)_2Ni(pin^F)]$ (**9**) in Et_2O.

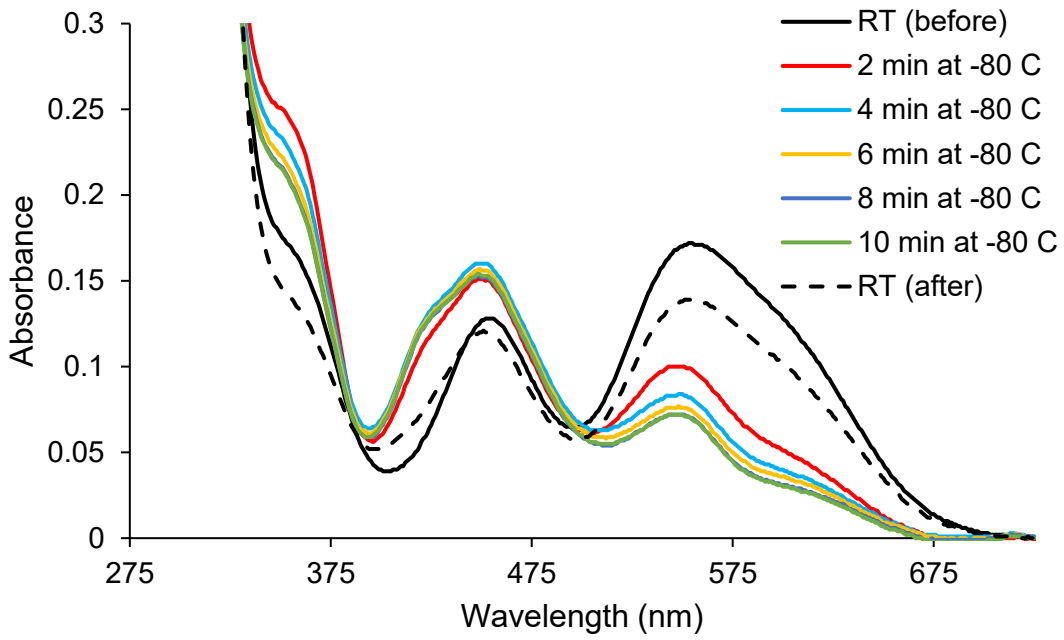

Figure 4. $[(Ph_3P)_2Ni(OC_4F_9)_2]$ (**3**) in THF starting at room temperature (black), cooled to −80 °C over 10 minutes (green).

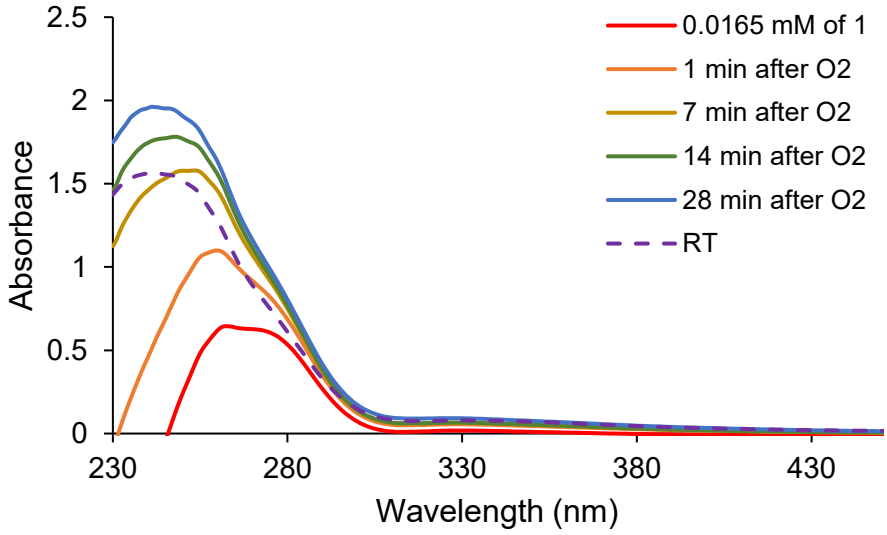

Figure 5. Reactivity of 0.0165 mM **1** in THF with O_2 over 28 minutes at −80 °C, and after reactivity at room temperature. At 28 minutes, λ_{max}= 241 nm, and the same wavelength is maintained upon warming to room temperature.

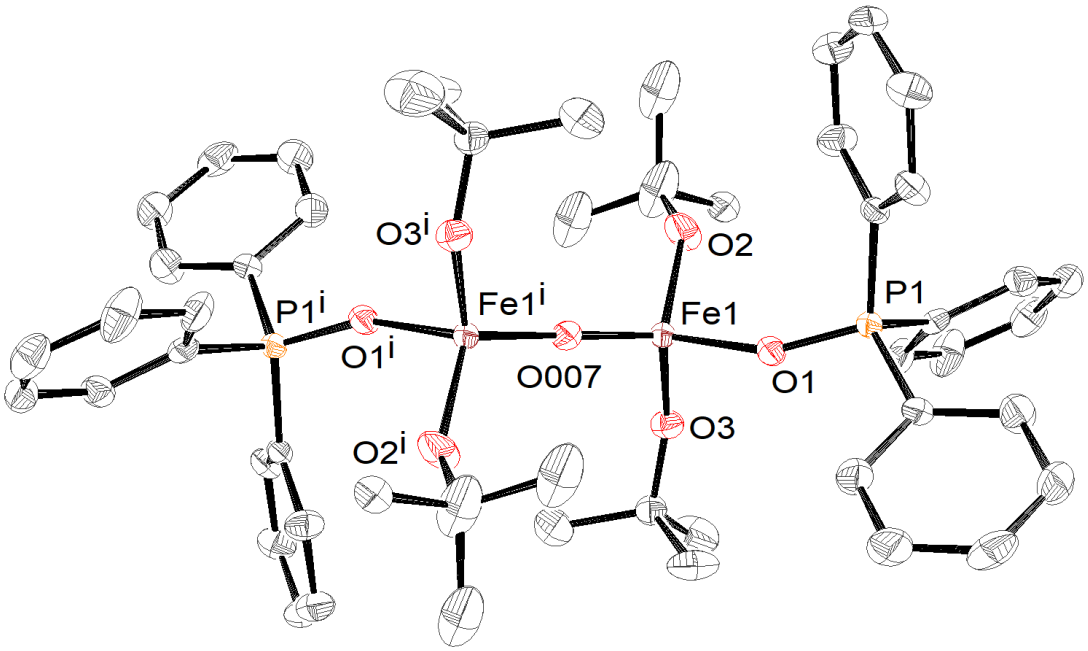

Figure 6. ORTEP diagram of **13**. Hydrogen and fluorine atoms were omitted for clarity. Ellipsoids are shown at the 50% probability level.